THE UNIVERSITY OF OKLAHOMA

GRADUATE COLLEGE

THE DETECTION OF NUCLEAR RADIATION USING THE CUMULATIVE PHOTODIELECTRIC EFFECT IN CADMIUM SULFIDE

A DISSERTATION

SUBMITTED TO THE GRADUATE FACULTY

in partial fulfillment of the requirements for the

degree of

DOCTOR OF PHILOSOPHY

BY

CHARLES WESLEY ALWORTH

Norman, Oklahoma

1969

THE DETECTION OF NUCLEAR RADIATION USING THE

CUMULATIVE PHOTODIELECTRIC EFFECT IN CADMIUM SULFIDE

APPROVED BY

C. R. Hoder

N B Hannay

H. T. Fischbeck

E. D. Hobbs

DISSERTATION COMMITTEE

ACKNOWLEDGMENTS

I would like to thank Dr. C. R. Haden who acted as chairman of my committee, and who gave many hours of valuable assistance. My thanks go to my wife who cajoled me through the writing of the dissertation. Finally, my thanks go to my mother who translated my handwriting, corrected my grammar, and typed both the rough draft and the reading copy.

TABLE OF CONTENTS

	Page
LIST OF ILLUSTRATIONS	v
LIST OF PLATES	vii
Chapter	
I. INTRODUCTION	1
II. PHYSICAL DEVELOPMENT	14
III. THE PHOTODIELECTRIC EFFECT	37
IV. PRELIMINARY EXPERIMENTAL DESIGN AND PREPARATION	60
V. EXPERIMENTAL TECHNIQUES AND INSTRUMENTATION	81
VI. RESULTS, CONCLUSIONS, AND RECOMMENDATIONS	91
BIBLIOGRAPHY	108
APPENDIX I	111
APPENDIX II	113

LIST OF ILLUSTRATIONS

Figure		Page
1-1.	Gas Characteristic	3
1-2.	The p-n Junction Detector	7
1-3.	Detection Oscillator of Borisov and Marinov	10
1-4.	The Re-entrant Cavity	12
2-1.	The Energy Spectra of the Alpha Particle	15
2-2.	The Energy Spectra of the Beta Particle	16
2-3.	Ionization as a Function of Distance for Alphas	18
2-4.	Pure Alpha Absorption Curve	18
2-5.	Idealized Pure Beta Absorption Curve	20
2-6.	Pure Gamma Absorption Curve	21
2-7.	Absorption Cross Sections for Lead	24
2-8.	The Zincblende Structure	25
2-9.	The Wurtzite Structure	26
2-10.	Temperature Dependence of the Bandgap Energy	27
2-11.	Band Structure for Sensitization	30
2-12.	Photoconductivity	32
2-13.	Photocurrent Effect	33
2-14.	Capture Cross Section versus Temperature	34
3-1.	$\Delta\epsilon_r'$ versus Binding Energy	50
3-2.	$\Delta\epsilon_r''$ versus Binding Energy	51
3-3.	Re-entrant Coaxial Cavity	53

LIST OF ILLUSTRATIONS (continued)

Figure		Page
3-4.	Variation of n with Time	58
4-1.	Sketch of the Experimental System	60
4-2.	The Re-entrant Cavity	61
4-3.	The Cavity	63
4-4.	Cavity Machine Drawing	64
4-5.	Cavity Cryogenic System	65
4-6.	A Transmission Line	67
4-7.	The Radioactive Source	75
4-8.	Counter Window	75
4-9.	Cavity G Factor Diagram	77
5-1.	Cavity Inside Its Dewars	83
5-2.	Instrumentation System Number 1	85
5-3.	Instrumentation System Number 2	86
5-4.	Instrumentation System Number 3	87
5-5.	Instrumentation System Number 4	88
6-1a.	Results of Run Number 1	92
6-1b.	Results of Run Number 2	92
6-2a.	Results of Run Number 3	93
6-2b.	Results of Run Number 4	93
6-3.	Results of Run Number 5	96
6-4a.	Results of Run Number 6	97
6-4b.	Results of Run Number 7	97
6-5.	Initial Characteristics of Source	98
6-6.	Characteristic of Source after Heating	98
6-7.	Foreshortened Cavity	99

LIST OF PLATES

Plate		Page
I.	General View of Experimental Apparatus	90
II.	View of the Cavity Header	90

THE DETECTION OF NUCLEAR RADIATION USING THE CUMULATIVE PHOTODIELECTRIC EFFECT IN CADMIUM SULFIDE

CHAPTER 1

INTRODUCTION

1.1 INTRODUCTION

This dissertation describes an investigation of the use of the photodielectric effect in semi-conductors for use as a nuclear radiation dosimeter. Presently, semi-conductor diode detectors and gaseous detectors are operated in the DC mode. In this mode, a DC electric field sweeps ionized charge carriers towards the electrodes, where they are collected and recorded. The scintillation detector depends on ionizing radiation causing a shift in the energy of electrons, which then return to their lower energy state, giving out light. This light must then be collected and recorded, using a photomultiplier tube. Since the semi-conductor and gaseous detectors rely on charge collection, a failure to collect all the ionized carriers will result in a loss of signal amplitude and resolution. In the case of the scintillation detector, failure to "see" all the light will also result in a loss of signal amplitude and resolution.

The photodielectric effect does not rely on charge collection, but on an induced change in the dielectric properties of the bulk semiconductor crystal.

There can be two types of dielectric change in a bulk semiconductor crystal, that which is short lived and that which exists over a long period of time compared to the measurement time. That is to say, a change will occur in the dielectric properties of the bulk so long as radiation is impinging on the crystal, but once the radiation stops, the dielectric constant of the bulk returns to the pre-radiation value. This type of change may be called temporary. The long term change can best be described as integration over time; as long as radiation impinges on the crystal the dielectric constant changes, but when the radiation stops, the dielectric constant remains at its final value. It is the latter case which is considered in the present work.

I.2 Background of Radiation Detectors

The present state of the art of nuclear radiation detectors includes three basic types of detectors: gaseous, semiconductor, and scintillation. The first two depend on ionized charge collection as their method of recording radiation, and the third depends on light collection.

The gaseous detector field may be divided into three sub-classes: ion chamber, proportional, and Geiger-Muller. These

types of detectors all use the simple principle that most radiation will naturally ionize a gas. Now if a gas is placed between two electrodes with a DC voltage applied to the electrodes, the ionized charge carriers caused by nuclear radiation will be collected and counted. Whether the system is an ion chamber, proportional, or Geiger-Muller depends on the voltage applied to the electrodes (see Figure 1-1).

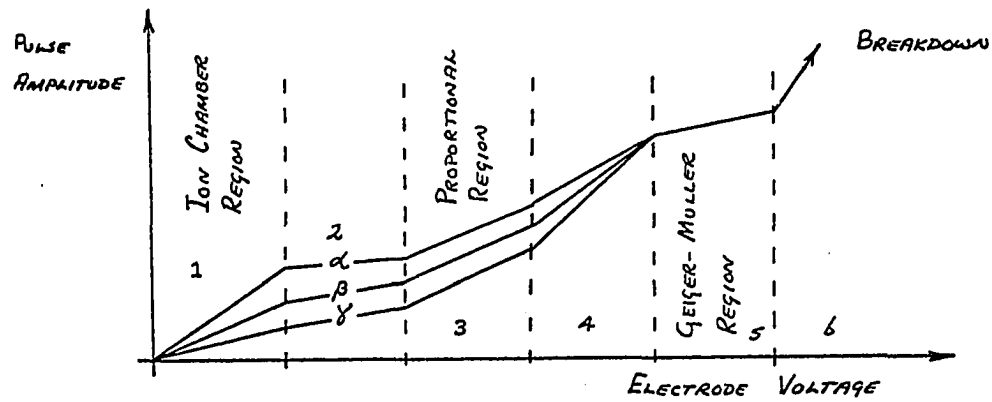

Figure 1-1. GAS CHARACTERISTIC

In the Geiger-Muller region, the voltage on the electrode is sufficiently high so that any primary ionization by nuclear radiation will produce cascade ionization resulting in a large signal output. The Geiger-Muller detector will respond to all types of ionizing radiation, but it will not give any information as to the energy content of the radiation, nor as to the type of radiation.

In the proportional region, the electrode voltage is high enough to produce secondary ionization, but cascade ionization will

not occur. Thus the output pulse is proportional to the primary ionization and thus proportional to the input radiation energy. This system works well for alpha and beta particles, but due to the low stopping power of gas, this system is practically useless for gamma ray energy studies.

Finally, the ion chamber detector is operated such that for each ionizing event, no secondary ionization occurs. This requires a low voltage on the electrodes. Because of the one event one charge principle (Appendix 2), the output of the ion chamber is so low that it is almost impossible to record. Thus if there is to be a practical or useful output, there must be many ionization events.

In addition to the inherent drawbacks, each of the latter two systems must have a very stable source of DC electrode voltage; otherwise voltage fluctuations will appear to be radiation events. Also, high amplification circuits must be used to amplify the output pulse or pulses. These circuits suffer from noise, as do the detectors themselves, resulting in a lower energy limit of about 1KeV. A further drawback is that the detectors become insensitive at high or low rates of radioactivity. At high flux rates, the gas does not have a chance to recombine between each of the events. Thus, the detector may see only one out of three (as an arbitrary figure) events; therefore, energy information at high rates of energy is impossible. At low flux rates, not enough events occur to be registered. Furthermore, a certain amount of energy is

needed to ionize a gas, and once the radiation energy falls below this level, no ionization of the gas can occur.

Scintillation detectors offer considerable advantages over gaseous detectors, principally because of the improved gamma ray characteristics. In this detector, radiation impinging on a crystal causes an upward shift in the energy of an electron. The electron then drops back to its lowest energy state, giving out light. Two types of luminescent emission in the phosphor must be distinguished. One is a delayed emission of radiation called phosphorescence, and the other is a direct process called fluorescence. The delaying process is caused by a shifting of the electron in its energy bands by subsequent radiation before it finally reaches the ground state. This delay can continue for 10^{-8} seconds or longer, whereas fluorescence takes place more rapidly. Consequently, a requirement for scintillation detectors is that the phosphorescence effect be minimal. A further requirement is that the crystal must be transparent to its own light. The light output must then be "seen" by a photomultiplier tube, and the resulting pulse must then be amplified. This process takes time, and thus lowers the time resolution of the detector, and due to the amplifiers, additional noise in the system is present.

Another disadvantage of the scintillation detector is that it exhibits poor alpha particle characteristics. This is due to the low ion conversion efficiency for excitation by heavily

ionizing particles. The poor conversion results from the fact that the alpha-particles excite electrons into the higher energy states which, because of their nature, do not give out light when they return to their lowest energy states. Finally, the system has a low energy limit of about 1KeV.

The advent of semiconductor detectors has resulted in considerable improvement over the gaseous and scintillation detector in many areas. Most semiconductor detectors rely on an ionizing event taking place in the depletion region of a p-n junction. There are basically three types of semiconductor: the p-n junction, the lithium drifted p-n junction, and the surface barrier. Each of these has a particular use. The p-n junction and lithium drifted p-n junction are used for beta detection, and the lithium drifted p-n junction may also be used for gamma-ray spectrometry.

The p-n junction detector is illustrated in Figure 1-2. The detector is essentially a reversed biased diode. This causes the depletion region to lie between 1 micron and 2000 microns, depending on the resistivity of the material and the amount of reverse bias. The 2000 microns (2 mm) depletion region may be obtained with 15K ohm-cm N type (or 40K ohm-cm P type) silicon, using a reverse bias of 1000 volts[13]. Unfortunately, as the reverse bias is increased, so is the noise level of the detector. At higher levels of reverse bias, the leakage (or reverse) current is

increased. The motion of these charge carriers causes noise.

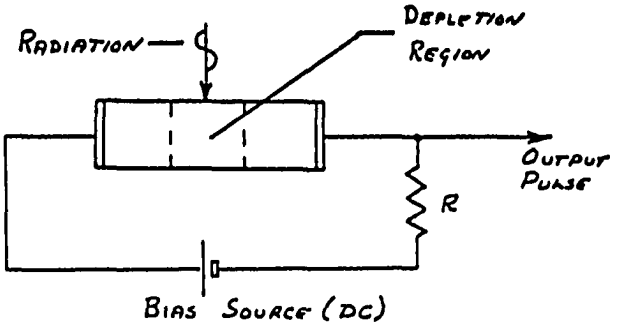

Figure 1-2. The p-n Junction Detector

The noise level limits the sensitive (depletion) region to about 1000 microns.[13] Detection is accomplished as radiation impinges on the crystal in the sensitive region, causing ionization. The high built-in electric field of a reverse-biased junction makes charge collection rapid, so that recombination noise is reduced. The p-n junction is formed using conventional diffusion doping techniques.

The surface barrier detector utilizes the surface properties of a semiconductor crystal to form a p-n junction, which is then reverse biased to form a large depletion layer. The barrier junction is formed by vacuum depositing a thin (2Å) of gold on the surface of a prepared chip of silicon. The sensitive thickness may reach 2mm. This larger depletion region means the detector can be used for beta-particles.

The lithium drifted detector is a p-n junction into which lithium ions have been diffused in order to compensate for impurities in the semiconductor crystal (silicon or germanium).

Using a lithium drifted semiconductor and normal p-n doping techniques, a detector may be obtained with a depletion region up to 15-20 mm wide. The drift process is explained by Pell.[39] Due to the larger depletion region, the lithium drifted detector may be used for gamma rays and beta particles.

The introduction of semiconductor detectors has resulted in an improvement over gaseous and scintillation methods. The energy resolution is improved, but the low energy limit is about 0.4KeV. Another drawback is the poor gamma ray efficiency of these devices, which arises because of the small depletion region of the p-n diode junction. The lithium drifted germanium detector has improved the gamma ray response, but the low energy cutoff is about 6KeV for gamma rays.[13] The lithium drifted germanium detector suffers from high background noise, so much so that it must be cooled in order to operate effectively. The high background noise results from the thermal motion of carriers in the germanium. This thermal motion has always been a problem in germanium.

Silicon lithium drifted detectors have improved noise characteristics, but have a low energy cutoff of 1MeV for gamma rays.[13] The improved noise characteristic at room temperature of the silicon detector is a direct result of the inherently lower noise characteristics of silicon. The cutoff arises because at 1 MeV, the pair-production process stops and the photoelectric process starts. Since the photoelectric absorption coefficient is related to the fifth power of the atomic number of the absorber, the coefficient is low for silicon as compared to germanium. In fact, the coefficient is approximately one-fortieth

that of germanium.

Another disadvantage of the semiconductor diode detector is charge collection; that is, all the charge caused by the ionizing event should be collected. The collection of charge is complicated by ion traps in the semiconductor crystal, statistical fluctuations in the amount of charge, and possible poor ohmic contacts to the bulk material. These factors cause spreading of the output pulse, and thus lower the energy resolution of the detector.

In nuclear radiation disometry high resolution is not needed, but the energy detector must be sensitive to all types of radiation. The basic limitations in sensitivity of particle detectors apply to dosimeters since a particle detector is used in conjunction with a dosimeter. That is, a particle detector is used to count radiation events, and electric circuits are used to integrate these events over time to a radiation dose. Since the low energy cutoff of the best devices is approximately 250eV, lower radiation energy would not be "seen" in present day dosimeters.

The AC mode offers exceptional advantages in that charge (ion or electron) collection is not necessary for the detector to operate. Because of this the AC mode offers low noise and high resolution as its properties. The high resolution is due to the fact that no time has to elapse for charge collection to occur, and only a few cycles of the AC field are needed to sense the change in the complex dielectric property of the detector, upon which the operation of the detector is based. Lower noise is obtained because of the lack of need for charge collection.

The low noise property of the AC mode could be used to detect very low energy radiation at very low flux rates. This would be very advantageous in the health physics field, and in radioisotope tracer techniques involving living organisms. (The high resolution property is not used in this work.)

1-3. Background of Previous Work in the AC Mode

The first work undertaken in the AC mode radiation detectors was done by Borisov and Marinov.[6] These researchers used a simple circuit arrangement in which a cadmium sulfide crystal was connected in parallel with the tuned circuit of an oscillator resonating at about one megahertz.

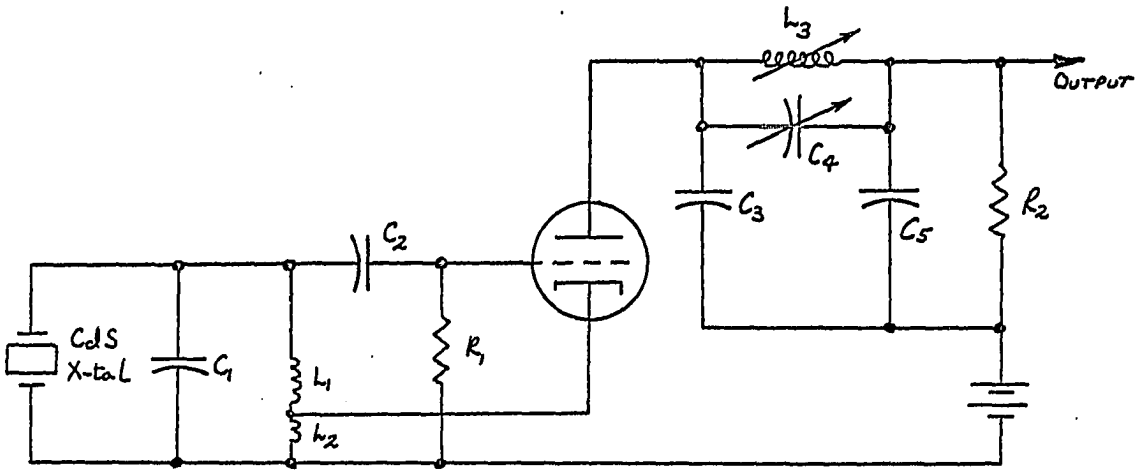

Figure 1-3. Detection Oscillator of Borisov & Marinov

Output pulses were seen through a low pass filter which eliminated the oscillator frequency. Thus, if radiation impinged on the crystal, there would be a change in the conductivity of the crystal, and an output pulse would appear at the output. Borisov and Marinov obtained the

energy spectrum of a known alpha source, with good correlation between the results of their experiment and the calibrated source.

Heimbecker[21] repeated the experiments of Borisov and Marinov, using CdS and alpha particles from Americium 241. Heimbecker proved that this method of radiation detection was feasible, but he did not obtain the same beautiful results of Borisov and Marinov. This was primarily because of the lack of signal processing equipment.

Neither of the experiments relied upon charge collection in order to obtain an indication of an ionizing event. However, due to the low frequencies involved, both experiments examined the change in crystal properties due to a single ionizing event. The crystal would return to its original state after the ionized charge carriers recombined. At higher frequencies the radiation would cause a detectable change in the complex dielectric properties of the crystal. This is known as the photodielectric effect.

1-4. The Photodielectric Effect

The photodielectric effect was first investigated by Arndt and Hartwig.[1,18] These researchers found that when silicon at 4.2°K was exposed to light, change in the complex dielectric constant occurred. Furthermore, it was found that this change was dynamic. That is, as the light intensity was changed, so did the complex dielectric constant change. The light source was a G-As semiconductor laser, whose intensity could be regulated by the applied bias voltage.

In the experimental work undertaken, a crystal of silicon was

placed on the stub of a 920 megahertz re-entrant cavity. The cavity was lead plated and cooled to $4.2^{o}K$, so that it became superconducting. The resulting high quality factor provided high frequency definition. This meant that any change in the dielectric properties of the silicon could easily be measured as reflected in a frequency change of the cavity. The cavity was operated as a transmission type, and measurements were taken of the change in cavity resonant frequency and transmitted power. With these measurements, the necessary information on the dielectric change could be determined.

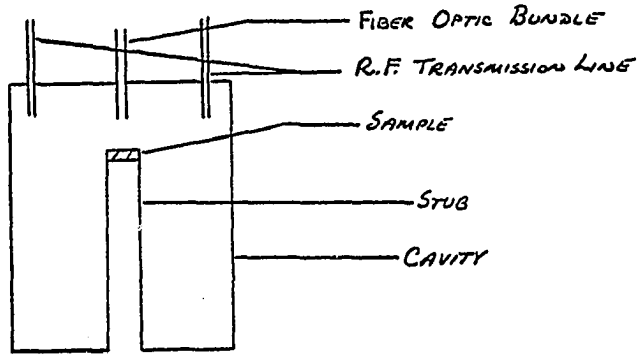

Figure 1-4. The Re-entrant Cavity

Further work on the photodielectric effect was undertaken by Hinds and Hartwig.[19,22] In this case, aluminum doped cadmium sulfide (CdS:Al) was placed on the stub of an 830 megahertz superconducting re-entrant cavity, and light was allowed to fall on the crystal. Optically induced electrons were transferred to the conduction band into which the electrons would fall. Previous work had shown that the lifetime of the electron traps in CdS:Al[22] could be very long. In all cases the lifetime was found to be of the order of days. When experimental work was done,

long lifetimes were found at 4.2°K. This trapping meant that over a period of time the dielectric properties of the crystal would change due to the light falling on the crystal. This effect on the dielectric properties can be called the cumulative photodielectric effect, and it is this effect which is herein investigated for possible use as a nuclear radiation detector.

CHAPTER 11

PHYSICAL DEVELOPMENT

2.1 Radiation

Radiation is the spontaneous emission of particles or energy at a well defined rate.[11] There are many types of radiation, including electrons, neutrons, positrons, the helium nucleus (H^{++}), or the alpha particle, all of which are particles. Other radiation includes X-rays and gamma rays which are electromagnetic energy and may be represented by photons.

Radiation may be divided into two types: ionizing radiation and non-ionizing radiation. The most common forms of ionizing radiation are alpha, beta (electrons), and gamma, which are the three types that concern the health physicist the most. An example of non-ionizing radiation is the neutron. All nuclear radiation arises from the radioactive decay of elements.

2.2 Radioactive Decay

There are many types of radioactive decay: alpha, beta, positron, electron capture, gamma emission, and internal conversion. In alpha decay, the atom emits a charged helium nucleus,

and changes to a different atom (the daughter), as described by

$$ {}_{Z}E^{A} \longrightarrow {}_{Z-2}E^{A-4} + \alpha $$

where Z is the atomic number and A is the atomic weight. E is the element undergoing disintegration. The resulting spectrum of the radioactive particles is mono-energetic, or it can have a few mono-energetic groups when the daughter nuclide can be left in one or more excited states. There is a lot of energy involved, since the energy of the alpha particles varies between 1.5 and 11MeV. However, the particle has a short range (up to 30 mm in air.)

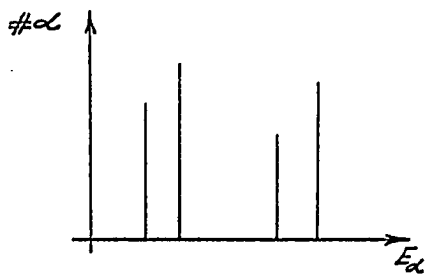

Figure 2-1. The Energy Spectrum of the Alpha Particle

In beta decay, the atom emits negatively charged electrons, with the result that the atomic mass remains the same, but the atomic number changes by plus one. At the same time, an anti-neutrino is emitted.

$$ {}_{Z}E^{A} \longrightarrow {}_{Z+1}E^{A} + \beta^{-} + \bar{\nu} $$

where Z, E, and A have previously been defined. β is a beta particle, and $\bar{\nu}$ is an anti-neutrino. The energy spectrum is continuous and has a maximum energy which varies from approximately 1KeV to 15MeV.

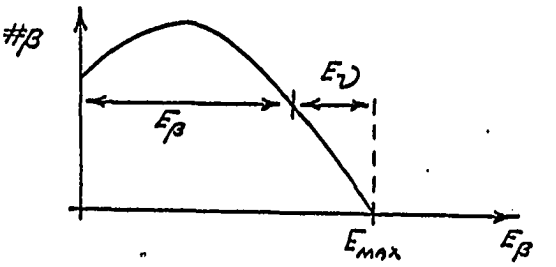

Figure 2-2. The Energy Spectrum of the Beta Particle

In positron decay, the atom emits positively charged electrons. The resultant energy spectrum is similar to that of beta decay. The atomic number of the daughter differs from the parent by minus one, and emits a neutrino. ($E_B > 2mc^2$ where E_B is the energy level difference.)

$$ {}_{Z}E^{A} \longrightarrow {}_{Z-1}E^{A} + \beta_{+} + \nu $$

where β_+ is a positive beta (positron) and ν is a neutrino.

A competing form of positron decay is electron capture, which is the capture by the nucleus of an orbital electron usually from the K-shell. This is followed by the emission of either one or more X-rays or an "Auger" electron, which is an electronic transition in an excited atom releasing enough energy for the ejection of a loosely bound electron without accompanying electro-magnetic radiation.

$$ {}_{Z}E^{A} + e \longrightarrow {}_{Z-1}E^{A} + \nu $$

where e is an electron ($E_B < 2mc^2$).

In gamma radiation, a nucleus goes from an excited state to a low energy state, or its ground state. Since these energy levels are discrete, the gamma spectrum will also be monoenergetic. Gamma radiation usually accompanies α, β_- or β_+ decay and is emitted almost simultaneously.

$$ {}_{Z}E^{A*} \longrightarrow {}_{Z}E^{A} + \gamma $$

Internal conversion serves as an alternative to gamma emission. In this process, there is an interaction of the nuclear field with one of the orbited electrons. This results in the emission of a series of mono-energetic electrons, whose energy will be the difference between the energy levels of the nucleus and the binding energy of the electron. This process is accompanied by X-rays as the orbital electrons shift energy levels.

2.3 Interaction of Ionizing Radiation With Matter

This discussion is concerned with three types of ionizing radiation: alpha, beta, and gamma. In the case of the alpha particle, the energy loss mechanism is primarily by interactions with the orbital electrons, resulting in decomposition, excitation, or ionization of the atoms, ions, or molecules of the radiated material. As the particle slows down and attains the same velocity as the K-shell electrons, the particle may pick up (and perhaps lose again) electrons from the absorbing material. At low velocities, the energy loss is by elastic collisions. An interesting point is that at high velocities, the specific ionization of the alpha particle is low because of the small interaction time, and at lower velocities, the specific ionization is high. This means that the alpha particle will lose energy constantly until the particle slows to a point where its interaction cross-section increases sharply. At this point the particle will give up its remaining energy rapidly. This is illustrated by Figure 2-3 on the following page.

Furthermore, if measurements of the number of alpha particles versus distance in a material are plotted, a range curve, such as Figure 2-4 (see following page) results.

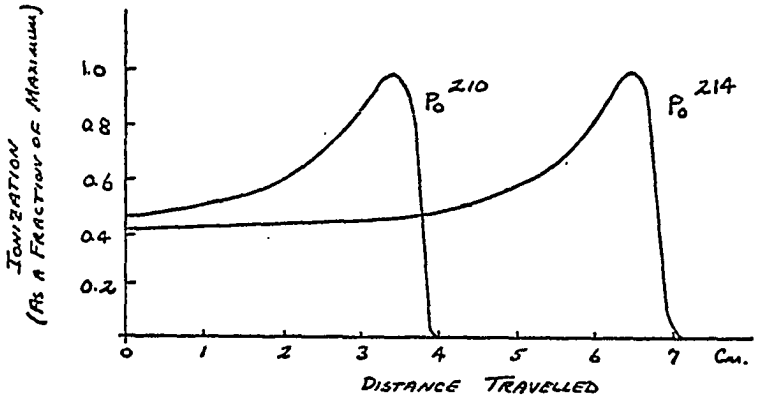

Figure 2-3. Ionization as a function of the distance a thin ionization chamber is placed from a source. While the range of Po^{214} alpha particles is much greater than that of Po^{210} alpha particles, the shape of the curves is very nearly the same. The ionization produced by a single alpha particle per unit length of length increases as the particle slows down.[24]

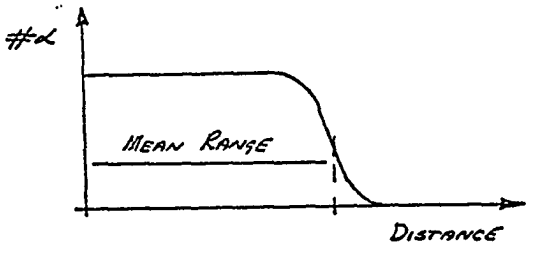

Figure 2-4. Pure Alpha Absorption Curve

This curve indicates that if the material of the absorber is thick enough, none of the alpha particles will fully penetrate the absorber. However, if the absorber is slightly thinner than the mean range, essentially all of the particles will penetrate it. An approximate equation for the range of alpha particles is given by[24]

$$R = k' \frac{Mv^3}{Z^2}$$

where k' is a constant of proportionality, M is the mass of the charge particle (in this case M is the mass of the alpha particle 4amu or 3278.171MeV/c^2), v is the velocity of the particle, and Z is the atomic number of the absorber.

In the case of beta particles, the process responsible for energy loss is qualitatively the same as for alpha particles. There are, however, the following important differences. First, the specific ionization is much less because of the smaller charge of the beta particles, i.e. the interaction cross section is smaller; thus there are fewer ion pairs generated per unit path length. Second, an electron may lose up to half its energy in a single collision. Third, there is pronounced scattering of the beam. Fourth, an electron may be accelerated in the field of a nucleus with the emission of bremsstrahlung (electromagnetic radiation) which is an important effect at high electron velocities and high absorber atomic number. Fifth and finally, since beta particles are emitted in a continuous energy spectrum, the beta particles are absorbed

at an almost exponential rate.

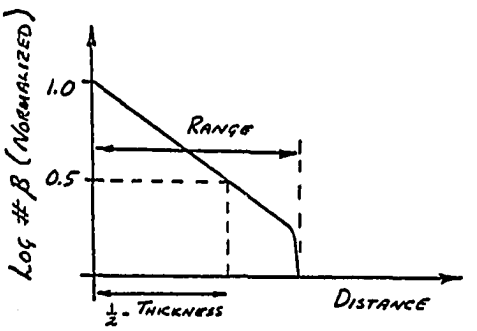

Figure 2-5. Idealized Pure Beta Absorption Curve

The range curve of Figure 2-5 shows that beta particles are absorbed at an exponential rate. For electrons with energy up to 10MeV, the dominant mode of energy loss is the same as that for alpha particles. An approximate range equation is given by[4]

$$R = \frac{4\pi e^4 ZN}{mv^2} B$$

where Z is the atomic number of the absorber, N is the number of absorber atoms per cm^3, v is the velocity of the beta particle, e is the charge of an electron, m is the mass, and B is the stopping number given by a formula due to Bethe.[13]

$$B = \ln(0.583mv^2)/I$$

where I is the mean ionization potential of the absorber atoms, v is the velocity, and m is the mass of the beta particle. At higher energies, the formula for B given by Muller[34] should be used. At energies above 10MeV, the bremsstrahlung mechanism is more important and the energy loss is proportional to Z^2NE_β,[13] where E_β is the energy

of the beta particle and N is the number of particles.

A gamma beam loses intensity as it passes through matter by elastic scattering of the photons, by the photoelectric effect, the Compton effect, pair production, nuclear absorption, and other processes that do not start until very high energies are reached. The last class will not be discussed. Each of the processes is important in a particular energy range for a given absorber, the energy range increasing roughly as the order given above. Because of these effects, gamma rays are attenuated with an exponential relationship as they pass through an absorber.

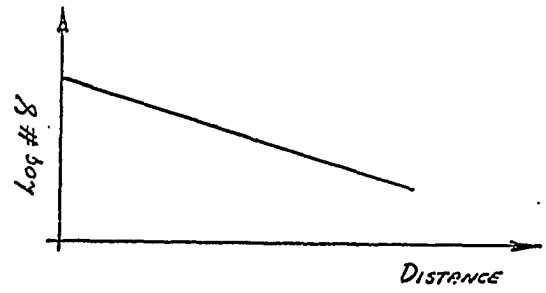

Figure 2-6. Pure Gamma Absorption Curve

Gamma rays may be scattered elastically by nuclei (Thompson scatter) or by atomic electrons (Rayleigh scatter). Thompson scattering is quite negligible except in the case of resonance scattering, which takes place in very special cases and is generally not important. Rayleigh scattering is appreciable, but small compared to the total attenuation of the intensity. The scattering angle is small, with the result that the scattered photons will still

penetrate the absorber. Furthermore, this effect tends to fall off as the energy of the photon increases. The effect is approximately proportional to Z/E, where E is the energy of the gamma photon.

In the photoelectric effect, the gamma ray gives up all its energy to the atom. The energy given to the ion is small, and the bound electron of the atom may be considered to have received the total energy of the gamma ray (or photon). The excited electron now has a kinetic energy given by $E - E_B$, where E_B is the binding energy of the electron to the atom. This effect is most important at low energies ($E_\gamma < 0.5$MeV) and high atomic number absorbers. The effect is approximately proportional to $Z^5/E^{7/2}$, for $E_\gamma < 0.5$MeV.

Compton scattering is the inelastic collision of a photon with orbital electrons (or any free electrons). In this event, the photon loses energy and is scattered as a photon of lower frequency, and the electron recoils with an energy equal to that lost by the photon. This effect is most important at medium energies of the gamma ray ($0.5 < E_\gamma < 1.5$MeV).

Pair production does not start until the energy of the gamma ray exceeds 1.02MeV.[24] In this effect, the gamma photon interacts with the nuclear field, forming a positive and negative electron pair as per the following equation.

$$E = h\nu_o = 2m_oc^2 + E_{\beta-} + E_{\beta+}$$

where $2m_oc^2$ is twice the rest mass energy of an electron, and $E_{\beta-}$ and $E_{\beta+}$ are the kinetic energies of the electron and positron

respectively. Very often, the positron and the electron will cause secondary ionization in the material. At thermal energies, the positron will combine with the electron and undergo annihilation, releasing two gamma rays of energy 0.51MeV each.

Finally, in photonuclear reactions, the gamma photon reacts with the nucleus; but in this case the energies involved are small because of the small interaction cross-section, and attenuation of the beam is negligible.

In all the processes, the number of photons absorbed, in a thickness dx of an absorber, is proportional to dx and to the intensity of the beam at that point. This leads to the expression

$$I = I_o e^{-ux}$$

in which the beam intensity I, after passing through a thickness x of absorber, is related to the initial intensity by the absorption coefficient u. This coefficient may be subdivided into

$$u = u_{photo} + u_{Compt} + u_{pair}$$

where each of these coefficients owes its existence to the effects already described. Figure 2-7 illustrates how the absorption coefficient varies with photon energy.

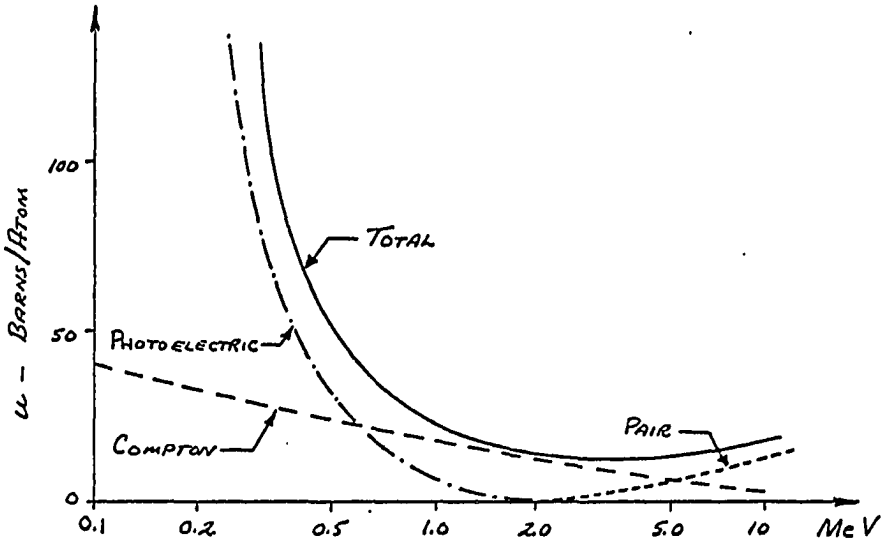

Figure 2-7. Absorption cross sections per atom of lead as a function of incident photon energy. The solid curve is the total absorption cross-section per atom for all three processes combined.[24]

2.4 The Crystal Structure of Cadmium Sulfide

Cadmium sulfide may crystallize into one of two forms, the zincblende structure or the wurtzite structure. Both of the structures are shown in Figures 2-8 and 2-9. In the zincblende structure, each atom is surrounded by four nearest neighbor atoms of the other kind, which are located at the vertices of a tetrahedron. In the sublattice of atoms of the same kind, there are twelve nearest neighbors. Six are located at the vertices of a hexagon surrounding the ionized atom; three more are above; and three more are below - all of which are located at the corners of a tetrahedron. There is no center of symmetry or inversion because of this

arrangement. The CdS layers have unique orientations. Zincblende crystals of CdS are polar, and opposed faces and opposed directions usually have different physical and chemical properties.

In the wurtzite structure, each cadmium atom is bonded to four sulphur atoms, located approximately at the corners of a tetrahedron. However, they do not have the same spacing. The twelve next nearest neighbors are arranged as in the zincblende structure. This structure may be viewed as two interlaced hexagonal close-packed lattices. The wurtzite structure, like the zincblende structure, has no center of symmetry or inversion. Either form of the crystal may be prepared, depending on the methods used. The zincblende will revert to the wurtzite structure when heated above 100°C, the wurtzite form being the stable form to 900°C.

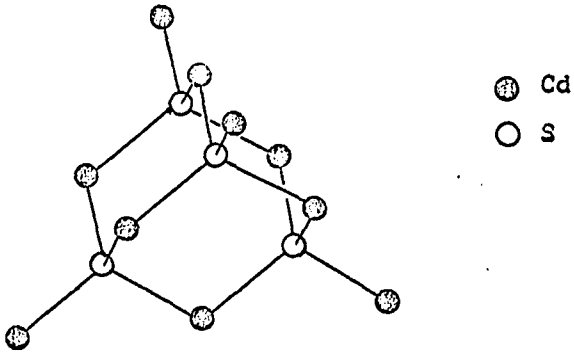

Figure 2-8. The Zincblende Structure

Due to the type of crystal structure, many of the physical properties of cadmium sulfide depend on the crystal orientation.

The properties of greatest concern in this study will be the dielectric constant, the energy bands, and the radiation absorption coefficient.

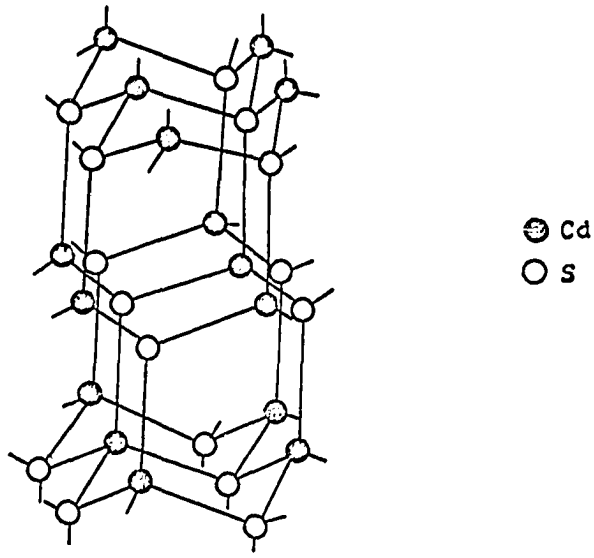

Figure 2-9. The Wurtzite Structure

2.5 Energy Band Structure of Cadmium Sulfide

The energy band structure of cadmium sulfide has been studied by a number of observers. A fairly complete picture may be found in a paper by Cardona and Harbeke.[10] In their dissertation, only the energy gap between the valence band and the conduction band is of interest. Data taken by various observers of the band gap energy result in the plot of E_g versus T in Figure 2-10.[12,29] Cardona and Harbeke give $E_g = 2.53$eV at 300°K, and Hopfield and Thomas[23] give $E_g = 2.5826$eV at 4.2°K.

The energy levels that appear in the band gap of cadmium

sulfide are well known, although the only levels that can be predicted with any degree of accuracy are the donor levels due to group III or VII impurities and those due to cadmium vacancies. Now, since the band gap energy varies with temperature, it can be assumed that the energy levels in the band gap will also vary with temperature.[29]

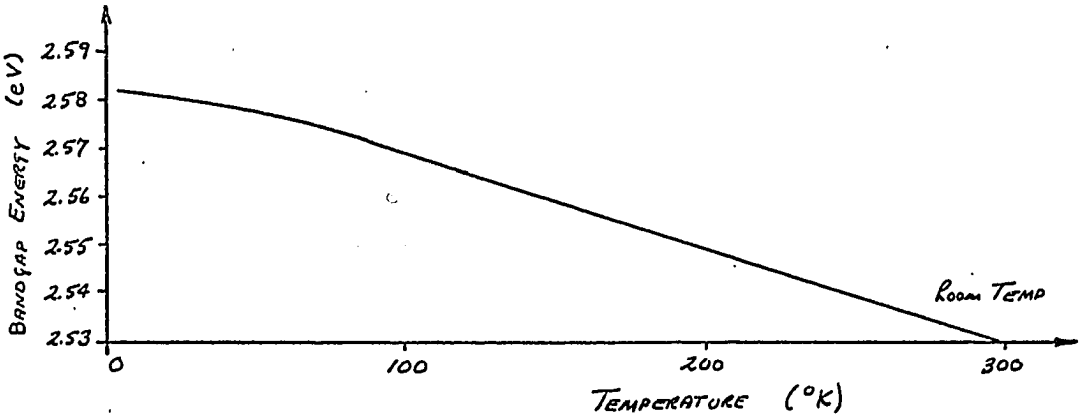

Figure 2-10. Temperature Dependence of the Bandgap Energy

The energy states between the valence band and the conduction band may be divided into two categories: traps and recombination centers. A center is classified as a recombination center if, on the average, carriers captured there have a higher probability of recombining, then being re-excited. A center is classified as a trap if the re-excitation probability is greater. These terms are defined at room temperature (300°K) and become somewhat vague at 4.2°K or lower. At low temperatures there is very little thermal energy, and consequently the probabilities of both recombination or re-excitation once an electron is in a center

is greatly reduced. Thus for the present purpose, a center will be called a trap if the center tends to capture and hold a carrier for a long time compared to the time it spends in the conduction band.

In semiconductors and insulators, traps and recombination centers are the results of imperfections in crystal lattice. There are many types of imperfections: two of the most common ones are foreign atom impurities, as intentional or unintentional doping, and crystal lattice defects. Free carriers and thermal motion may also be termed imperfections, but these do not contribute permanent discrete levels in the forbidden band.

No single crystal is perfect, since the surface itself is a departure from the perfect crystalline structure. Other imperfections, almost guaranteed in a crystal, are edge and screw dislocations, which involve planes of atoms, Schottky defects which involve discrete atoms or ions, Frenkel defects, vacancies, and interstitials. The methods by which these defects are generated is explained in most solid state physics texts.[44] Other defects are discussed in Kittel.[26] Thus in nominally pure cadmium sulfide there will always be energy levels in the forbidden band.

According to Bube,[8] anion (sulfur) vacancies act as donors, and cation (cadmium) vacancies act as acceptors. It is fairly easy to adjust the stoichiometry of CdS crystals.[45] Woods[45] found that excess cadmium may be achieved (removal of sulfur) by heating a

crystal in vacuum up to 700°C. Colbow[12] annealed crystals for 24 hours at 539°C under equilibrium cadmium vapor pressure.

Generally, acceptor sites are common in most cadmium sulfide crystals. However, donor sites depend for the most part on doping. A great amount of speculation is involved in assigning energy levels to various imperfections; for instance, the level due to silver doping claimed by Lambe[30] to be about 0.4eV is disputed. Bube[7] states that traps with a level of 0.4eV are characteristic of the cadmium sulfide crystal. However, it is generally agreed that cadmium vacancies generate hole traps about 1.0eV above the valence band, and III and VII impurities generate donor levels at approximately 0.03eV below the conduction band.[2] Other impurity effects in cadmium sulfide involve various substances absorbed on the surface, such as oxygen and water vapor.

2.6 Sensitization of Cadmium Sulfide

Cadmium sulfide is a good photodetector because it may be sensitized by impurity incorporation. Rose[42] discusses the methods of sensitization, and it involves the concept of compensated cadmium vacancies, which are cadmium vacancies containing one or two captured electrons. Assume that there exists a crystal with electron traps at a level E_a as shown in Figure 2-11a. Also assume that the sites are partially filled with electrons.

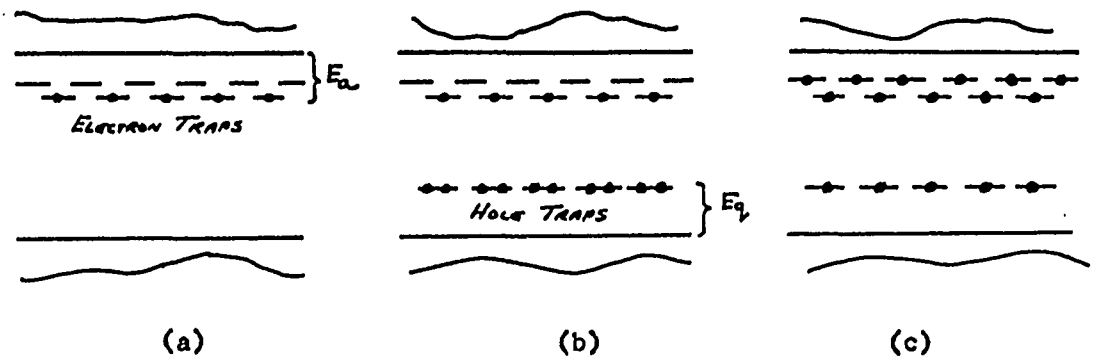

Figure 2-11. Band Structure for Sensitization

Now allow a number of compensated vacancies to be introduced. Since each vacancy has two captured electrons, it has a double negative charge due to the absence of the $C_{d^{++}}$ ion. This results in an energy level E_q above the valence band, which is illustrated in Figure 2-11b. Leaving the energy levels in this state, assume that radiation energy falls on the crystal; the energy takes electrons from the valence band to the conduction band. Under normal circumstances, the electrons would suffer recombination at one of the centers located in the forbidden band. Due to the nature of the cadmium vacancies, which will be called quenching sites, the expected recombination does not occur. In fact, the quenching sites have a large capture cross-section for holes, since they themselves have already captured two electrons. Thus, they will immediately capture the hole created by the radiation event. This now reduces the charge at the site to minus one. This means that the electron formerly in the quenching site is now located in the

valence band, while the electron formerly in the valence band is now in the conduction band, where it drops into the traps just below the conduction band. Furthermore, the quenching site is still negatively charged, leaving the capture cross-section for electrons quite small. Thus the free electron tends to be captured at the activation site, which is illustrated in Figure 2-11c. Notice that the net effect of the radiation is to transfer, irreversably, electrons from the quench site to the activation level.

This model is considered to be the correct model for sensitized cadmium sulfide. The activator element, in the case of this work, is aluminum (CdS:Al) which provides electron traps located close to the conduction band. As explained earlier, there are always a number of trapping levels even without intentional doping. Furthermore, it should be evident that the presence of the conduction or valence bands is not required, since it is possible to transfer electrons directly between the quench and activator levels, if the levels are physically located close to each other.

Investigations concerned with the senzitization of cadmium sulfide have centered on the effects of light on the conductivity. With this in mind, and also the model discussed, consider a special case of doping in which $N_q \gg N_a$, i.e., there are fewer activator levels than quenching levels. As soon as light falls on the crystal (note how easily this may be applied to radiation),

electron-hole pairs are created. The holes are immediately trapped, and the electrons begin filling the trap located at the activator level. These traps will eventually become full, and the electrons will begin to fill the conductor band, since the holes are still being trapped at the quenching site. If no recombination is assumed, a large density of electrons can be held in the conduction band. Finally, after the quenching sites are filled, the holes would then be available for recombination, and no more electrons would be held in the conduction band. This procedure can be represented graphically by the plot of Figure 2-12, which assumes constant incident energy.

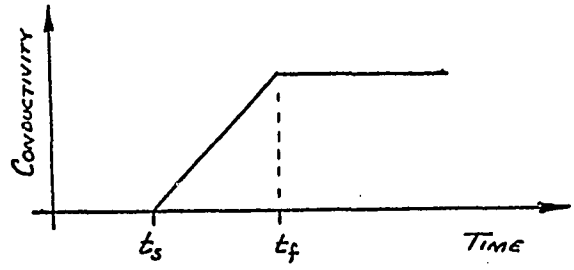

Figure 2-12. Photoconductivity

The first portion represents the time that the hole and electron traps are being filled. During this time, no appreciable change in the number of free electrons can be expected. At time t_s the electron traps will be filled, and the electrons will now start to fill the conduction band. At time t_f the hole traps will have been filled, and recombination of the electron-hole pairs will begin. Thus, the conductivity will no longer change.

In the preceding discussion, recombination has been ignored. It can be seen that at low temperatures if an electron is excited into an activation site, the probability of escape is very low (low thermal energy). Thus this neglect of the effect of recombination is valid. Several researchers[15,16,31] have reported effects of this nature, terming them "storage". These effects were generally noticed as a persistent photocurrent once the light source has been turned off. This is illustrated in Figure 2-13.

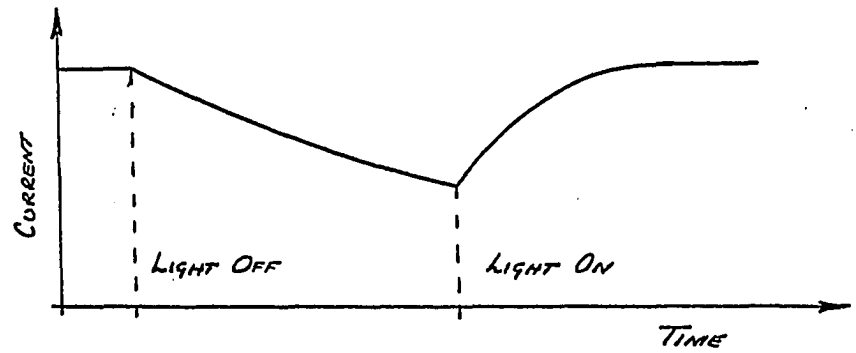

Figure 2-13. Photocurrent Effect

Further details may be found in references 27, 28 and 31.

2.7 Other Factors affecting Storage-Resetability

The previous discussion concerned a model which contains only enough features to explain a few experimental results. Other optical phenomena occuring in cadmium sulfide must also be explained. This explanation must be consistent with the model already offered. Many experimenters have noticed a decay in the photocurrent at

various temperatures. Generally, the current begins to decay very rapidly at about 200°K, while it is more or less constant below 200°K. This is strange because it is known that the holes are securely trapped up to about 400°K. Now in order for the photo-current to drop, the electrons in the conduction band have to combine with free holes which are not available.

One explanation presented by several investigators looks at electron traps which are known to be present, but do not seem to fill when the temperature becomes low. One such trap would not fill below 180°K,[9] another trap would not fill below 210°K.[47] A simple explanation follows. Assume that there are electron traps available in the crystal which have small cross-sections at very low temperatures. Now assume that as the temperature increases, the capture cross-section increases very slowly until the temperature reaches 200°K. At 200°K, a critical point is reached, at which the capture cross-section increases sharply.

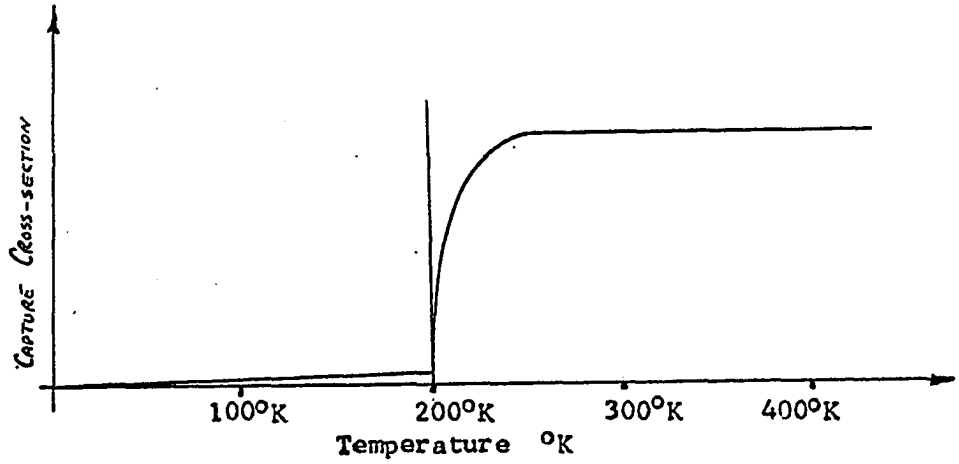

Figure 2-14. Capture Cross-Section vs Temperature

This means that at above 200°K, these traps will fill, with the result that not so many electrons are available for conduction. This means that a cadmium sulfide crystal can effectively be reset to zero (i.e.all storage removal) by heating it to above 200°K. This presents a straightforward way of resetting the crystal at low temperatures.

Another interesting effect is infrared quenching in which a crystal is illuminated long enough to obtain the persistent photocurrent (storage). Once this is obtained, the light should be shut off, and light of a lower wave length allowed to fall on it.[7] This light lowers, or quenches, the photocurrent. It is believed that the lower wave length light forces the holes in the quench sites to drop into the valence band, thus freeing them for recombination.[32]

The "tap effect" is also associated with the freeing of trapped holes. In this case, if the crystal is tapped, the photocurrent is decreased. Here the mechanical vibration of the crystal produces phonons, which in turn stimulate the holes, freeing them for recombination. This effect can be useful for resetting the crystal at low temperatures.

Finally, there is some evidence that the trapped holes may be released by applying a suitable electric field to the crystal. Dussel and Bube[14] have analysed the various mechanisms by which this process may occur, and Kallman and Mark[25] have demonstrated that

zinc sulfide and zinc-cadmium sulfide may be de-excited by high AC and DC electric fields.

Thus it is possible to reset the crystal by application of optical, mechanical, or electrical means. This means that either case may be useful or detrimental. The methods can be useful in the case of wanted resetability; detrimental in the case of unwanted resetability. Thus during an experimental run, care should be taken that the crystal is not reset accidently by one of the processes explained.

CHAPTER III

THE PHOTODIELECTRIC EFFECT

3.1 The Macroscopic Constant

In the macroscopic description of the dielectric properties of a substance, the principal parameter is the dielectric constant ϵ (farad/m). This parameter appears in equations used to describe the effects of electromagnetic waves in a substance and even appears in the expression for capacitance. The dielectric constant can be changed by various methods such as heating the substance, exposing the substance to radiation (light or nuclear), and placing the crystal in a high electric field. By the photodielectric effect, it is understood that the change in the dielectric constant arises because of light photons. This principle can be extended to a change in the dielectric constant due to nuclear radiation.

The underlying concept of the dielectric constant from an atomic viewpoint is that of an electric dipole moment. For a system of charged particles, the dipole moment is defined as[38]

$$\vec{p} = \sum_i q_i \vec{r}_i \qquad (3\text{-}1)$$

where q_i is the charge associated with the i-th particle and $\vec{r}_i$

is the displacement of that particle with respect to the origin. In an electrically neutral system, $\vec{p}$ as defined by equation (3-1) is independent of the origin of the system. As proof, suppose that the origin is shifted by a vector displacement $\vec{r}_o$, thus the dipole moment in the new system becomes

$$\vec{p}' = \sum_i q_i(\vec{r}_i + \vec{r}_o) = \sum_i q_i\vec{r}_i + \vec{r}_o\sum_i q_i = \vec{p} \qquad (3\text{-}2)$$

This follows since the summation of the charge must be zero, because the substance is space charge neutral.

The macroscopic counterpart of $\vec{p}$ is the electric polarization $\vec{P}$, which appears in the auxiliary Maxwell equation as follows:

$$\vec{D} = \epsilon_o\vec{E} + \vec{P} \qquad (3\text{-}3)$$

where $\vec{D}$ is the electric flux density (coul/m^2), $\vec{E}$ is the electric field (volt/m), and ϵ_o is the dielectric constant of free space (farad/m). Furthermore, the macroscopic $\vec{P}$ is the volume average of the dipole moment $\vec{p}$. An elegant proof appears in Wang,[44]

$$\vec{P} = \sum_i \frac{q_i\vec{r}_i}{V} \qquad (3\text{-}4)$$

where V is volume. Remembering that

$$\vec{D} = \epsilon_o\epsilon_r\vec{E} \qquad (3\text{-}5)$$

and substituting equation (3-5) in (3-3) gives

$$\vec{P} = \epsilon_o\left[\epsilon_r - 1\right]\vec{E} \qquad (3\text{-}6)$$

then equating equations (3-4) and (3-6) yield

$$\epsilon_r = \frac{1}{\epsilon_o V |E|} \sum_i q_i \vec{r}_i + 1 \qquad (3\text{-}7)$$

where V is the volume and $|E|$ is the applied field. Thus it appears that the relative dielectric constant is related to the applied electric field and to the displacement of each charge, assuming a non-linear displacement versus $\vec{E}$ is possible.

3-2 Change in the Relative Dielectric Constant

The equation of motion for a charged particle in any type of force field may be written as

$$m \frac{d^2\vec{r}}{dt^2} + B \frac{d\vec{r}}{dt} + k\vec{r} = \vec{F} \qquad (3\text{-}8)$$

where m is the mass, B is the damping or loss constant, k is the restoring force constant, and $\vec{r}$ is the displacement vector. In this equation, the first term represents the acceleration force, the second gives the viscous damping force, and the third is the elastic binding force. When an alternating electric field in the x-direction is taken to be the applied force, the preceding equation may be written as

$$m \frac{dx^2}{dt^2} + B \frac{dx}{dt} + kx = qE'\epsilon^{jwt} \qquad (3\text{-}9)$$

where $E'\epsilon^{jwt}$ is the internal field. If the material is highly polarizable, then local field corrections are not necessary.[36,37]

The resonant frequency of a harmonic oscillator is

$$w_o = \sqrt{\frac{k}{m}} \tag{3-10}$$

A solution of (3-9) gives

$$x = \frac{(q/m)E'\epsilon^{jwt}}{-w^2 + jwB/m + w_o^2} \tag{3-11}$$

The above equation may be rationalized to yield

$$x = \frac{[(q/m)E'\epsilon^{jwt}][(w_o 2 - w^2) - jwB/m]}{[(w_o^2 - w^2)^2 + (wB/m)^2]} \tag{3-12}$$

Since the applied field is in the x-direction and the field is $E = E'\epsilon^{jwt}$, then equation (3-7) may be modified to yield

$$\epsilon_r = \frac{1}{\epsilon_o V E'\epsilon^{jwt}} \sum_i q_i x_i + 1 \tag{3-13}$$

Now allow the x variation of equation (3-12) to apply to each charge; furthermore, substitute equation (3-12) into (3-13) to obtain the following

$$\epsilon_r = \sum_i \frac{q_i^2}{m_i V \epsilon_o} \left[\frac{(w_{oi}^2 - w^2) - jw/\tau}{(w_{oi}^2 - w^2)^2 + (w/\tau)^2} \right]_i + 1 \tag{3-14}$$

where $\tau = m/B$, and is in fact the momentum relaxation time.
The above equation describes the dielectric constant. However, the function of interest is the change in the dielectric constant.

Equation (3-14) may be simplified by taking the summation over a per unit volume. Thus the volume dependence may be removed, and equation (3-14) becomes

$$\epsilon_r = \sum_i \frac{q_i^2}{m_i \epsilon_o} A_i + 1 \qquad (3\text{-}15)$$

where the substitution

$$A = \left[\frac{(w_{oi}^2 - w^2) - jw/\tau}{(w_{oi}^2 - w^2)^2 + (w/\tau)^2} \right] \qquad (3\text{-}16)$$

has been made.

Since the change in dielectric constant is the matter of importance, the charge position vectors that do not change will be separated from equation (3-16). This means that only the moving charge carriers affect the dielectric constant. These carriers may be represented by a new class "t". Therefore equation (3-15) becomes

$$\epsilon_r = \sum_k \frac{q_k^2}{m_k \epsilon_o} A_k + 1 + \sum_t \frac{q_t^2}{m_t \epsilon_o} A_t \qquad (3\text{-}17)$$

where k = i-t, and is the class which contributes nothing to the change in the dielectric constant.

In the case of cadmium sulfide, the only charge carriers causing the dielectric change are electrons, since these are the carriers that are being trapped. Electrons have the same mass and charge; therefore the mass and charge in the last term of equation

(3-17) are replaced by e and m. Also it follows that w_{ot} is simply w_o, and equation (3-17) may be written

$$\epsilon_r = \sum_k \frac{q_k^2}{m_k \epsilon_o} A_k + 1 + \frac{e^2}{m\epsilon_o} nA \qquad (3\text{-}18)$$

where A has been defined, and n is the density of free electrons.

Now if some of the electrons are trapped, then there will be a change in the free electron density, or if some of the trapped electrons are released, there will be a density change. It is apparent from equation (3-18) that the change in dielectric constant may be written

$$\Delta\epsilon_r = \frac{e^2}{m\epsilon_o} \Delta n \, A(w, w_o) \qquad (3\text{-}19)$$

where Δn is the net change in electron density, and $A(w,w_o)$ is $[(w_o^2 - w^2) - jw/\tau] / [(w_o^2 - w^2)^2 + (w/\tau)^2]$. It is implicit that Δn is a negative number because the change in density is due to trapping. Thus the electron contribution to the dielectric constant may be represented by a constant term, independent of the excitation, plus a term that changes under excitation.

$$\epsilon_{r_e} = \epsilon_{r_o} + \Delta\epsilon_r \qquad (3\text{-}20)$$

where ϵ_{ro} is given by the first two terms in equation (3-18).

When the value of $A(w,w_o)$ is substituted into equation (3-19), $\Delta\epsilon_r$ is given by

$$\Delta\epsilon_r = \frac{e^2\ \Delta n}{m\epsilon_o}\left[\frac{(w_o^2 - w^2) - jw/\tau}{(w_o^2 - w^2)^2 + (w/\tau)^2}\right] \qquad (3\text{-}21)$$

which is complex.

Thus

$$\epsilon_r = \Delta\epsilon_r' + j\Delta\epsilon_r'' \qquad (3\text{-}22)$$

where

$$\Delta\epsilon_r' = K\Delta n\left[\frac{w_o^2 - w^2}{(w_o^2 - w^2)^2 + (w/\tau)^2}\right] \qquad (3\text{-}23)$$

and

$$\Delta\epsilon_r'' = K\Delta n\left[\frac{w/\tau}{(w_o^2 - w^2)^2 + (w/\tau)^2}\right] \qquad (3\text{-}24)$$

and $K = e^2/m\epsilon_o$. The basic form of these equations is similar to the complex polarizability. In general, as the electrons shift energy levels, the value of w_o and τ will also change. All that remains now is to calculate the value of w_o , Δn, and τ.

As previously stated, the frequency of a classical oscillator w_o is given by

$$w_o = \sqrt{k/m}\ . \qquad (3\text{-}25)$$

The restoring force on an oscillator with displacement y is given by

$$F = ky. \qquad (3\text{-}26)$$

The potential energy of this system is

$$W = \tfrac{1}{2} w_o^2 \, my^2 . \tag{3-27}$$

The total energy of the oscillator is obtained when y is a maximum and when the kinetic energy is zero.

$$W_{max} = \tfrac{1}{2} w_o^2 \, my_{max}^2 \tag{3-28}$$

Coulombs' law gives the attractive force between two charges

$$F = \frac{1}{4\pi\epsilon_o} \frac{q_1 q_2}{r^2} \tag{3-29}$$

where r is the separation, and q_1 and q_2 are the magnitudes of the charges involved. When the charges are equal and opposite and of magnitude e, the above equation becomes

$$F = \frac{1}{4\pi\epsilon_o} \frac{e^2}{r^2} \tag{3-30}$$

The maximum potential energy is given by equation (3-31)

$$W = \frac{1}{4\pi\epsilon_o} \frac{e^2}{y_{max}} \tag{3-31}$$

from which the value of y_{max} may be obtained.

$$y_{max} = \frac{1}{4\pi\epsilon_o} \frac{e^2}{W} \tag{3-32}$$

Equation (3-32) may now be substituted into equation (3-30) to obtain w_o in terms of W, the potential energy in Joules.

$$w_o^2 = \frac{2W^3 \left[4\pi\epsilon_o \right]^2}{e^4 m_e} \tag{3-33}$$

where m_e is the effective mass (see Appendix II) of the electron. The above equation reduces to

$$w_o^2 = (1.7)(10^{29})\frac{(m)}{(m_e)} E^3 \qquad (3\text{-}34)$$

where E is the potential energy in electron volts. The energy of electron traps is measured from the conduction band. Reference to equation (3-23) shows that as w, the electric field frequency, approaches w_o, then $\Delta \epsilon_r$ approaches zero. In fact, $\Delta \epsilon_r$ is identically equal to zero when $w = w_o$. An estimate of w_o may be made by allowing E to be 0.03eV, which is the energy level for cadmium sulfide,[12] and m_e/m to be 0.2, which is the correct value for cadmium sulfide.[2] With these values, w_o becomes 765 GHz, and thus w will be less than w_o. w is the frequency of the applied electric field, since w_o is 765 GHz and for this work w is 400 MHz, thus w will be less than w_o.

The term Δn, which is the net change in density of the free electrons, must now be explained. This can be done by using a simple model that involves a density change between two energy levels, due to an applied stimulus. This would mean that in the case of cadmium sulfide, electrons are being transferred from their normal free state to the trap site. Thus $\Delta n_2 = -\Delta n_1$; which means that a certain number of electrons leave state 1 and enter state 2. The density change is also proportional to the time that the electron spends in the trapped state ; thus the expression for the density change becomes

$$\Delta n = f_t \tau_t / V \qquad (3\text{-}35)$$

where f_t is the rate at which the electrons are excited into the trap, and τ_t is the average time the excited electrons spend in this trap. V is the sample volume. This equation represents the steady-state value of Δn under the condition that electrons are excited into the trap. If, however, the electrons are excited out of the trap, then

$$\Delta n = -\bar{f}_t \bar{\tau}_t / V \tag{3-36}$$

where $\bar{\tau}_t$ represents the average time the electron spends out of state t, and $\bar{f}_t$ is the rate at which electrons are excited. In this case, Δn is a positive quantity.

The generation rate f_t is related to the radiation intensity and the absorption coefficient for the type of radiation. Thus, in general

$$f_t = \alpha \phi \tag{3-37}$$

where ϕ is the radiation flux intensity, which is sufficiently energetic to cause a shift in electron levels, and α is a conversion coefficient, which when multiplied by ϕ gives the number of electrons transferred. Thus the net change of electron density Δn becomes

$$\Delta n = \alpha \phi \tau_t / V \tag{3-38}$$

where V is the sample volume.

In the case of cadmium sulfide, τ_t approaches infinity, which presumes that an infinite change in electron density is possible. This in fact is not true, and equation (3-38) should be used to

represent a change in Δn due to an increment of ϕ. Thus the total change in Δn may be obtained by integrating the increment of ϕ; thus

$$\Delta n = \frac{\alpha}{V}\int_0^t \phi\,(t)\,dt \tag{3-39}$$

where $\phi(0) = 0$. This equation does not allow for saturation which comes about because there are a finite amount of trapping sites available in cadmium sulfide. Once these trap sites have been filled, no further change in Δn can take place. This topic is discussed in a later section.

This discussion shows that if radiation impinges on a crystal of cadmium sulfide under the proper temperature conditions, a change in the dielectric constant results. The same discussion applies if the excitation stimulus is light, as Hinds has shown.[22] Thus

$$\Delta\epsilon_r = \frac{e}{m\epsilon_o}\left[\frac{\alpha'}{V}\int_o^t \phi\,(t)\,dt\right]\left[\frac{w_o^2 - w^2 - jw/\tau}{(w_o^2 - w^2)^2 + (w/\tau)^2}\right] \tag{3-40}$$

The next term to be discussed is τ, which is the momentum relaxation time. Nussbaum[38] shows that the mean time between free electron collisions, τ_e, and τ are essentially the same. Kittel[26] gives the following relationship for τ

$$\tau = m_e u/e \tag{3-41}$$

where u is the carrier mobility, m_e is the effective mass, and e is the charge.

If u is taken as $10 cm^2/volt\text{-}sec$[13], with m_o/m equal to 1, then τ becomes $(5.7)(10^{-15})$. If w is $(2.5)(10^9)$, then w/τ is $(4.4)(10^{23})$, which is fairly small when compared to w_o^2 , $[\doteq (4.6)(10^{24})]$. This value of τ is really a lower limit (actually the value of τ used is that for hole mobility at 300^oK, and electron mobility, even at 4.2^oK, will be higher than this value), thus w/τ would become smaller and may therefore be neglected. Thus equations (3-19) and (3-20) may be written as

$$\Delta\epsilon_r' = K\Delta n \left[\frac{1}{w_o^2 - w^2}\right] \tag{3-42}$$

$$\Delta\epsilon_r'' = K\Delta n \left[\frac{w/\tau}{(w_o^2 - w^2)^2}\right] \tag{3-43}$$

A close look at the above equations shows that the change in the complex dielectric constant is only a function of n_t and w_o, since the operating frequency (w) is being kept relatively constant. This is the frequency of the applied electric field, which is changing by only a few KHz in 400 MHz. However, w_o is really a function of E, which will be investigated later; thus the change in dielectric constant is related to the radiation flux intensity and the absorption properties of the crystal.

3.3 The Effect of the Binding Energy on the Dielectric Constant

In the preceding section, the change in dielectric constant is found to be a function of time (for long life traps), the number of

of electrons, the intensity of radiation, and w_o. That is

$$\Delta\epsilon_r = f(t, w_o, n, \phi) \tag{3-44}$$

Now when the dependence on t,n, and ϕ is neglected, then $\Delta\epsilon_r'$ and $\Delta\epsilon_r''$ may be written

$$\Delta\epsilon_r' = K\left[\frac{w_o^2 - w^2}{(w_o^2 - w^2)^2 + (w/\tau)^2}\right] \tag{3-45}$$

$$\Delta\epsilon_r'' = K\left[\frac{w/\tau}{(w_o^2 - w^2)^2 + (w/\tau)^2}\right] \tag{3-46}$$

where $K = e^2/m\epsilon_o$.

Equation (3-45) may be plotted as a function of E, the binding energy appearing in equation (3-34). Assume the previous value of τ and w, $[(5.7)(10^{-15})$ and $(2.5)(10^9)$ respectively$]$, then substitution of equation (3-34) and these values of w and τ into equation (3-41) yields

$$\frac{\Delta\epsilon_r'}{K} = \frac{(1.7)(10^{29})E^3}{(2.9)(10^{58})E^6 + (1.94)(10^{47})} \tag{3-47}$$

This is plotted in Figure 3-1.

If equation (3-45) is differentiated, then the maximum value of $\Delta\epsilon_r'$ occurs when $w_o^2 = w^2 + w/\tau$, which for this sample calculation occurs when E = 0.014eV. This value is fairly close to the value of E for aluminum doped cadmium sulfide given in the literature.[12]

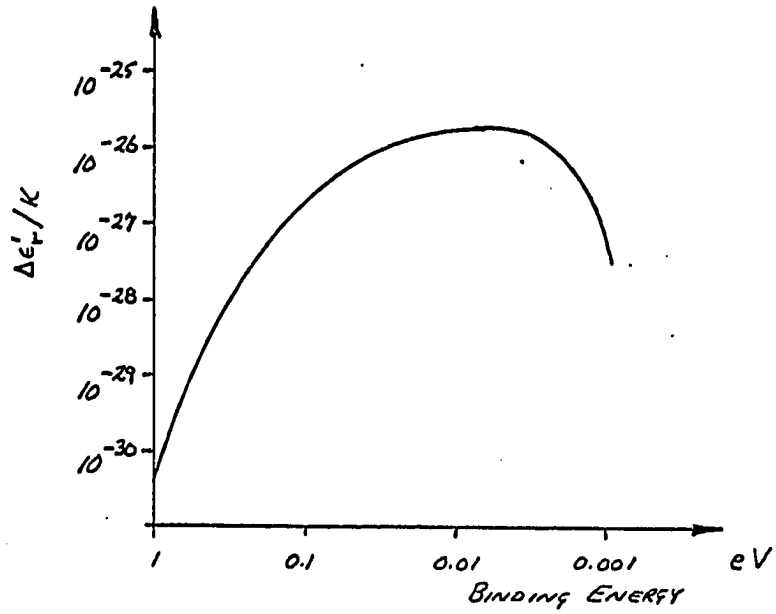

Figure 3-1. $\Delta\epsilon_r'$ versus Binding Energy

Note that these calculations assume m_e/m equal to 1 and r equal to $(5.7)(10^{-15})$, which is not truly accurate.

Notice that as E approaches zero, or as $w^2 >> w_o^2$, the electron begins to behave like a free electron, and the change in the real part of the dielectric constant becomes

$$\Delta\epsilon_r' = \frac{e^2 n}{m_e \epsilon_o} \frac{1}{w^2 + 1/\tau^2} \tag{3-48}$$

This is the same as Arndt's[1] equation for the change in the real part of the dielectric constant brought about by exciting electrons from the valence band to the conduction band.

Equation (3-46), the imaginary portion of the relative dielectric change, may also be calculated as a function of E.

Assuming the same values of w and τ used in obtaining equation (3-47) and again using equation (3-34) and substituting them into equation (3-46), the following is obtained.

$$\Delta\epsilon_r'' = \frac{(4.4)(10^{23})}{(2.9(10^{58})E^6 + (1.94)(10^{47})} \qquad (3\text{-}49)$$

This is plotted in Figure 3-2. Note that $\Delta\epsilon_r''$ changes rapidly, then levels off.

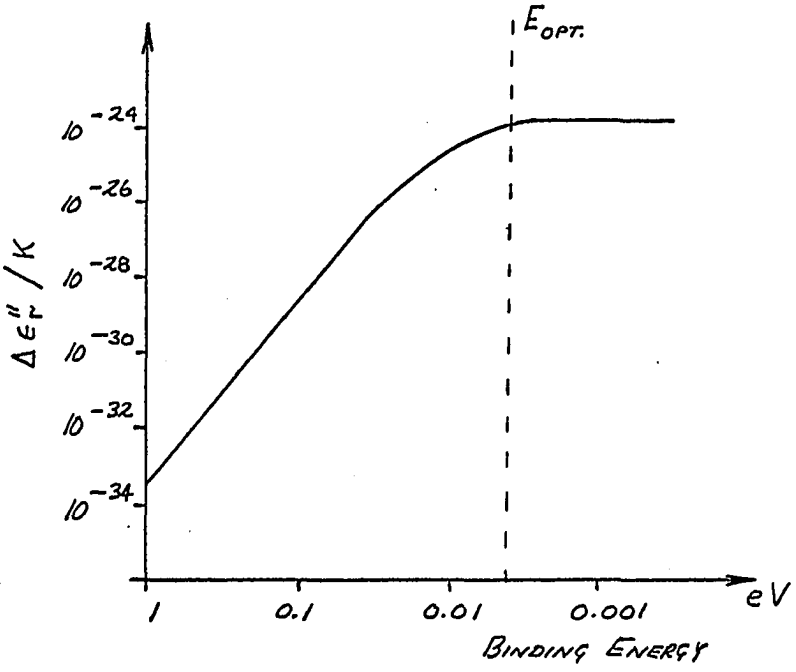

Figure 3-2. $\Delta\epsilon_r''$ versus Binding Energy

Equation (3-49) may be simplified. In the case of deep traps, $w_o \gg w$, then the change in the imaginary portion of the dielectric constant can be written

$$\Delta\epsilon_r'' = \frac{w/\tau}{w_o^2} \tag{3-50}$$

In the case when the traps are shallow, $w>w_o$, then the equation becomes

$$\Delta\epsilon_r'' = \frac{w/\tau}{(w/\tau)^2} = \frac{\tau}{w} \tag{3-51}$$

Hence it is evident that the imaginary portion has a small value for deep electron traps, and rises to a higher constant value as the traps become shallower. In the sample calculation previously worked, it was shown that $E_{OPTIMUM}$ was 0.014eV. For this value of E, the imaginary portion has reached its maximum value.

Equation (3-46) can be reduced to the free electron value when w_o approaches zero, or as E approaches zero.

$$\Delta\epsilon_r'' = \frac{e^2 n}{m_e \epsilon_o} \frac{\tau/w}{w^2\tau^2 + 1} \tag{3-52}$$

which is the same result as was obtained by Arndt.[1]

3.4 Cavity Perturbation Theory

A good way to measure changes in the dielectric properties of a crystal is to place the crystal in a high Q resonant cavity and measure the change in frequency and quality factor (Q) due to the change in the dielectric constant. The cavity chosen for this work was a re-entrant coaxial cavity, with the sample placed on the tip of

the re-entrant stub as shown in Figure 3-3.

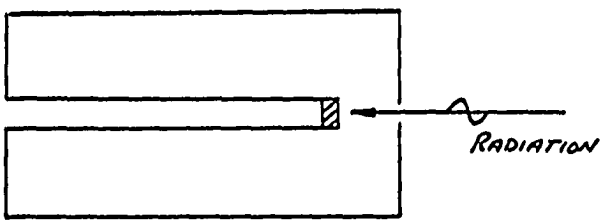

Figure 3-3. Re-entrant Coaxial Cavity

According to perturbation theory, changes in the dielectric constant of a sample in a cavity will show up as changes in the cavity resonant frequency and quality factor. The use of a high Q superconducting cavity will show these changes in frequency more markedly and will allow precise measurements to be made. Arndt[1] has analysed the cavity perturbation problem, and only the highlights of his results will be used.

The complex angular frequency, w, for a resonant cavity can be written

$$w = w' + jw'' \tag{3-53}$$

where w' is the real component and is determined by the real frequency, and w'' is the imaginary component. The relationship between the complex angular frequency to the real frequency and quality factor has been determined for a complex perturbation to be[43]

$$\frac{\Delta w}{w_1} = \frac{w_1 - w_o}{w_1} = \frac{f_{r_1} - f_{r_o}}{f_{r_1}} + j\left[\frac{1}{2Q_1} - \frac{1}{2Q_o}\right] \tag{3-54}$$

where w_o is the original frequency in radians per second, w_1 is the new frequency in radians per second, Q_o is the value of Q associated with w_o, Q_1 is the new value, f_{r_1} and f_{r_o} the frequencies in hertz. Thus there are two components for a change of resonant frequency of a cavity. The real part is

$$\frac{\Delta w'}{w_1} = \frac{f_{r_1} - f_{r_o}}{f_{r_1}} \tag{3-55}$$

and the imaginary part is

$$\frac{\Delta w''}{w_1} = \frac{1}{2}\left[\frac{1}{Q_1} - \frac{1}{Q_o}\right] \tag{3-56}$$

Hence the change in dielectric constant can produce two effects in the operating characteristics of the cavity.

It may be shown[1] that, for a high Q superconducting cavity, the initial change in resonant frequency when the sample is placed on the stub is given by equation (3-57), where ϵ_c is the dielectric constant of the crystal ($\epsilon_r = \epsilon_c/\epsilon_o$), V_s is the sample volume, and V_c is the cavity volume.

$$\frac{\Delta w_a}{w_1} = \frac{\epsilon_o - \epsilon_c \int_{V_c} \epsilon_o |E|^2 dV}{\epsilon_o \int_{V_s} (\epsilon_o \vec{E}^2 + \mu_o \vec{H}^2) dV} \tag{3-57}$$

The right side of equation (3-57) is not easily evaluated for the present geometry, but if ϵ_c is known, then the value of the ratio of the two integrals may be determined experimentally. Hence

$$K = \frac{\int_{V_c} \epsilon_o |E|^2 \, dV}{\int_{V_s} (\epsilon_o E^2 + \mu_o H^2) \, dV} \tag{3-58}$$

The value of K is constant for any given sample and cavity. Therefore the change in frequency may be written as

$$\frac{w_a}{w_1} = \frac{\epsilon_o - \epsilon_c}{\epsilon_c} K \tag{3-59}$$

Now if the dielectric constant of the crystal should now become ϵ_c', then a similar expression may be written for the change in frequency when the sample is placed in the cavity.

$$\frac{\Delta w_b}{w_1} = \frac{\epsilon_o - \epsilon_c'}{\epsilon_c'} K' \tag{3-60}$$

If the change in dielectric constant has not affected the cavity fields, then K and K' are equal.

Therefore the change in frequency obtained when the crystal dielectric constant changes from ϵ_c to ϵ_c' is given by

$$\frac{\Delta w}{w_1} = \frac{\Delta w_a - \Delta w_b}{w_1} = \frac{\epsilon_o(\epsilon_c' - \epsilon_c)}{\epsilon_c' \epsilon_c} K \tag{3-61}$$

Since the changes in the dielectric constant will be small, then $\epsilon_c \epsilon_c' \simeq \epsilon_r^2 \epsilon_o^2$. Therefore

$$\frac{\Delta w}{w_1} = \frac{\Delta \epsilon_r}{\epsilon_r^2} K \tag{3-62}$$

where $\Delta \epsilon_r$ is the change in relative dielectric constant. Note that as ϵ_r increases, w decreases.

In a previous section, it was shown that the change in relative dielectric constant could be written as

$$\Delta\epsilon_r = \Delta\epsilon_r' + j\Delta\epsilon_r'' \tag{3-22}$$

Hence the change in the cavity frequency may be written as

$$\frac{\Delta w}{w_1} = \frac{K}{r^2}\left[\Delta\epsilon_r' - j\Delta\epsilon_r''\right]. \tag{3-63}$$

But this change may also be written as

$$\frac{\Delta w}{w_1} = \frac{f_{r_1} - f_{r_2}}{f_{r_1}} + j\left[\frac{1}{2Q_1} - \frac{1}{2Q_2}\right] \tag{3-54}$$

$$\frac{\Delta w}{w_1} = \frac{w_1 - w_2}{w_1} + j\left[\frac{1}{2Q_1} - \frac{1}{2Q_2}\right]. \tag{3-64}$$

Furthermore, Arndt [1] shows that

$$Q = \frac{-w}{2\Gamma} \tag{3-65}$$

where w is the frequency and Γ is the absorption coefficient. Thus, the change in frequency may be written as

$$\frac{\Delta w}{w_1} = \frac{w_1 - w_2}{w_1} + j\left[\frac{\alpha_2}{w_2} - \frac{\alpha_1}{w_1}\right]. \tag{3-66}$$

Comparison of equations (3-66) and (3-63) shows that the change in the real portion of the complex dielectric constant affects only the resonant frequency of the cavity, whereas a change in the imaginary portion affects the quality factor, or the power absorption. The expression for power absorption in a dielectric constant is given by

$$P_{ABS}\frac{1}{2} = w\epsilon_2'' E^2 \tag{3-67}$$

where E is the electric field.

3.5 Saturation

It has been shown in a previous section that the change in the real part of the complex relative dielectric constant is a function of time, the number of electrons changing state, the radiation flux intensity, and w_o. That is

$$\Delta\epsilon_r' = f(t, w_o, \Delta n, \phi) \tag{3-44}$$

The effect of w_o on the value of $\Delta\epsilon_r'$ has been explored, but the effects of time, the number of electrons changing state, and the radiation flux have not. These three terms arise because of the dependency of $\Delta\epsilon_r'$ on the net change of density of the free electrons (Δn). That is

$$\Delta\epsilon_r' = K_t \Delta n \tag{3-68}$$

where $K_t = K\Lambda(w, w_o)$, which is a modification of equation (3-23). For the case of long lifetime traps

$$\Delta n = \frac{\alpha}{V_s}\int_0^t \phi(t)dt \tag{3-39}$$

It should be obvious that after a period of time, the electron traps will fill, and no further change of Δn will occur; hence no further change in $\Delta\epsilon_r'$ will occur. The relationship between time and the number of traps filled (hence Δn) should be almost linear. This is because the electrons are being placed in "compartments", or that the

repulsive forces between the trapped electrons are small. Only when the trap sites (or compartments) are almost full would the repulsive forces begin to have an effect. Hence the change in electron density would appear as shown in Figure 3-4.

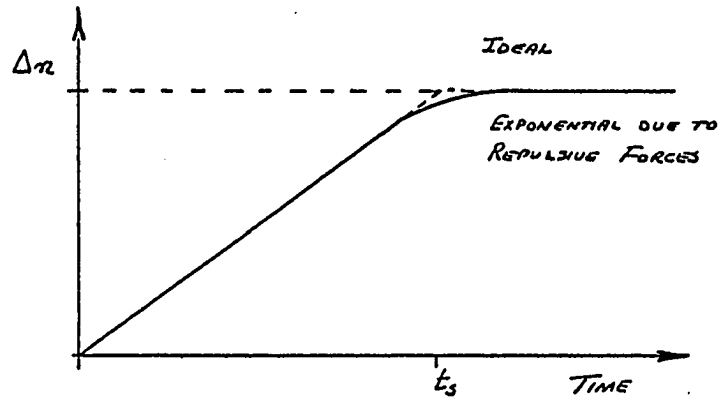

Figure 3-4. Variation of Δn with Time

Furthermore, the maximum value of Δn would be equal to n_t, the density of trap sites available in the crystal.

Now allow t_s to be the time at which saturation occurred. Thus

$$\Delta n_{max} = \frac{\alpha}{V}\int_0^{t_s} \phi(t)dt = n_t \tag{3-69}$$

or since ϕ (t) = constant

$$\phi\, t_s = \frac{n_t V}{\alpha} \tag{3-70}$$

Now if the radiation flux is constant, then

$$t_s = n_t V/\alpha\phi \tag{3-71}$$

where ϕ is the radiation intensity.

As an example, assume 156 KeV beta particles with an activity of approximately one microcurie. A quick glance at Figure 2-2 shows that this would be a maximum value of beta energy; hence, assume that the average energy of the beta particle is 100 KeV. Furthermore, since the bandgap is 2.53 eV, assume that 2.53 eV is required to put an electron in a trap. The number of electrons transfered due to one beta particle will be $(3.95)(10^4)$ electrons per event. Now since one microcurie source emits $(3.7)(10^4)$ particles per second, the total number of electrons transfered will be $(1.46)(10^9)$ electrons per second.

Now assume that the trap sites are due only to the aluminum doping. The molecular weight of CdS is 144.46 and the density is 4.82; therefore, there are $(2.01)(10^{22})$ molecules per cubic centimeter. The doping level is 0.0264%; therefore, the number of aluminum atoms is approximately $(5.3)(10^{18})$ atoms per cubic centimeter. This compares favourably with the results obtained by Hinds[22] for his CdS:Al crystal. The sample volume will be given by

$$V = d^2h/4 \qquad (3\text{-}72)$$

where d is the diameter (0.79 cm) and h is the thickness (0.2 cm) of the crystal. Thus the sample volume is 0.1 cc. All the quantities in equation (3-71) are now known and the saturation time is

$$t_s = \frac{(5.3)(10^{18})(0.1)}{(3.95)(10^3)(3.7)(10^4)} = (2.10)(10^4) \text{ hours} \qquad (3\text{-}73)$$

which is an extremely long time. Thus at low energies and intensities of radiation, saturation of the dielectric constant change should cause no problems.

CHAPTER IV

PRELIMINARY EXPERIMENTAL DESIGN AND PREPARATION

4.1 Introduction

The experimental system may be divided into two basic parts, the cavity with its sample, and the associated instrumentation. The instrumentation consisted of various oscillators, spectrum analysers, and the like, which were used to measure changes in the cavity operating characteristics. The cavity and sample really form the more important part of the experimental system. These must be cooled to the temperature of liquid helium. The experimental system is sketched in Figure 4-1, and will be explained in the following sections of this chapter.

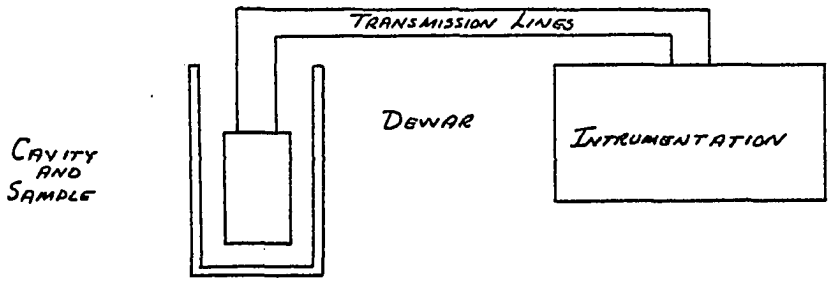

Figure 4-1. Sketch of the Experimental System

4.2 Design of the Cavity and Transmission Lines

As explained in chapter three, a change in dielectric constant can be measured using a high Q cavity. As the cavity resonant frequency is made higher, the cavity dimensions are reduced, and the crystal may become a larger part of the cavity volume. The larger the volume that the crystal occupies, the greater the effect of the change in dielectric constant on the cavity resonant frequency. However, if the crystal occupies too much volume, it would have a tendency to load the cavity and cause the results of the perturbation theory to be inaccurate. An operating frequency of 400 MHz was chosen mainly because of equipment limitations, and also because, at this frequency, a re-entrant cavity would have convenient dimensions to fit in a Dewar.

Ramo, Whinney, and Van Duzer[40] discuss the re-entrant cavity or foreshortened coaxial line, shown in Figure 4-2a. This cavity may be considered as a coaxial line, A, terminated in the gap capacitance B, leading to the equivalent circuit of Figure 4-2b.

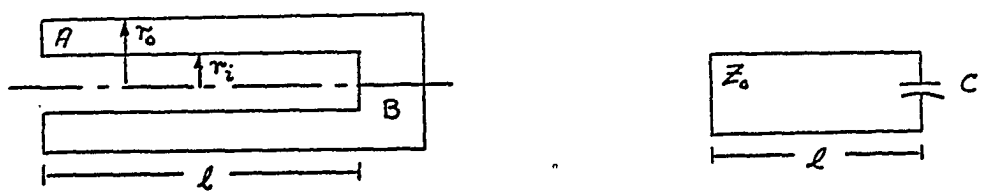

a b

Figure 4-2. The Re-entrant Cavity

This model holds, provided that region B is small compared to the wave length. If the gap capacitance is smaller, then l is $\lambda_o/4$, where λ_o is the resonant wave length. For a resonant frequency of 400 MHz, λ is 75 centimeters. Hence l is 18.75 centimeters. The distance B between the re-entrant post and the cavity end was held up to 3/8 inch (0.953cm), which meant that the design requirement $B \ll \lambda$ was satisfied.

The Microwave Engineers' Handbook[20] states that the quality factor of a re-entrant cavity would be optimized if the ratio $r_o:r_i$ was made equal to 3.6. Hence, once the value of r_o was chosen, then r_i was set, since the optimum (maximum) Q was desired. The value of r_o chosen was 5/8 inch (1.588cm), which meant that the outer wall of the cavity would be made of 1-3/8 inch brass pipe. This pipe has an ID of 1-1/4 inches. The limitation on the external diameter of the cavity was set by the available helium Dewar which had a neck diameter of 1-1/2 inches. With the value of r_o set, the re-entrant stub could be turned out of brass stock to a diameter of 3/8 inch, thus obtaining the optimum ratio $r_o:r_i \simeq 3.6$ (in this case $r_o:r_i$ was 3.34).

A prototype cavity was then built, using copper tubing which approximated the values of r_o and r_i required. This cavity was literally thrown together, but in spite of the poor construction techniques, its resonant frequency was 395 MHz (400 MHz required.) This cavity was first operated as a reflection type, but results were difficult to obtain, and it was found that the transmission type worked better.

The top end plate of the cavity was made larger than needed (electrically) so that it could hold a radioactive source. An instep of 5/8 inch diameter was drilled in the cavity end plate, and covered with a removable disc which had a 1/8 inch diameter hole in the center. This disc would hold the radioactive source in place and allow radiation to impinge on the crystal. Because of the geometry of the instep and its covering disc, some correction on the amount of radiation striking the crystal must be made. This is explained in a later section of this chapter.

The top end plate was designed to fit snugly into a channel on the side wall of the cavity. This channel could then be filled with molten Woods metal, which upon solidifying would form a good seal and make the cavity vacuum tight. The top end plate was attached to the two 5/16 inch ID stainless steel support tubes, which were in turn attached to a header. Figure 4-3 shows the assembled cavity, and Figure 4-4 shows a machine drawing of the side view of the cavity.

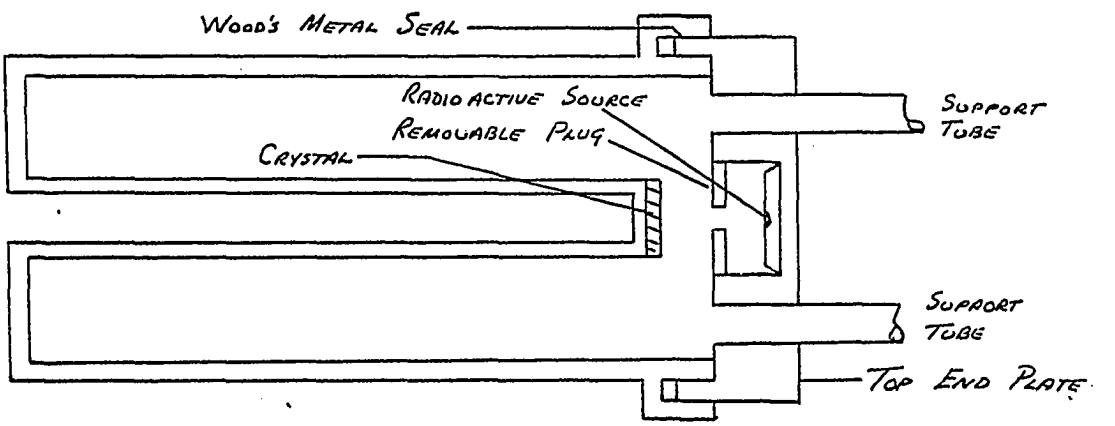

Figure 4-3. The Cavity

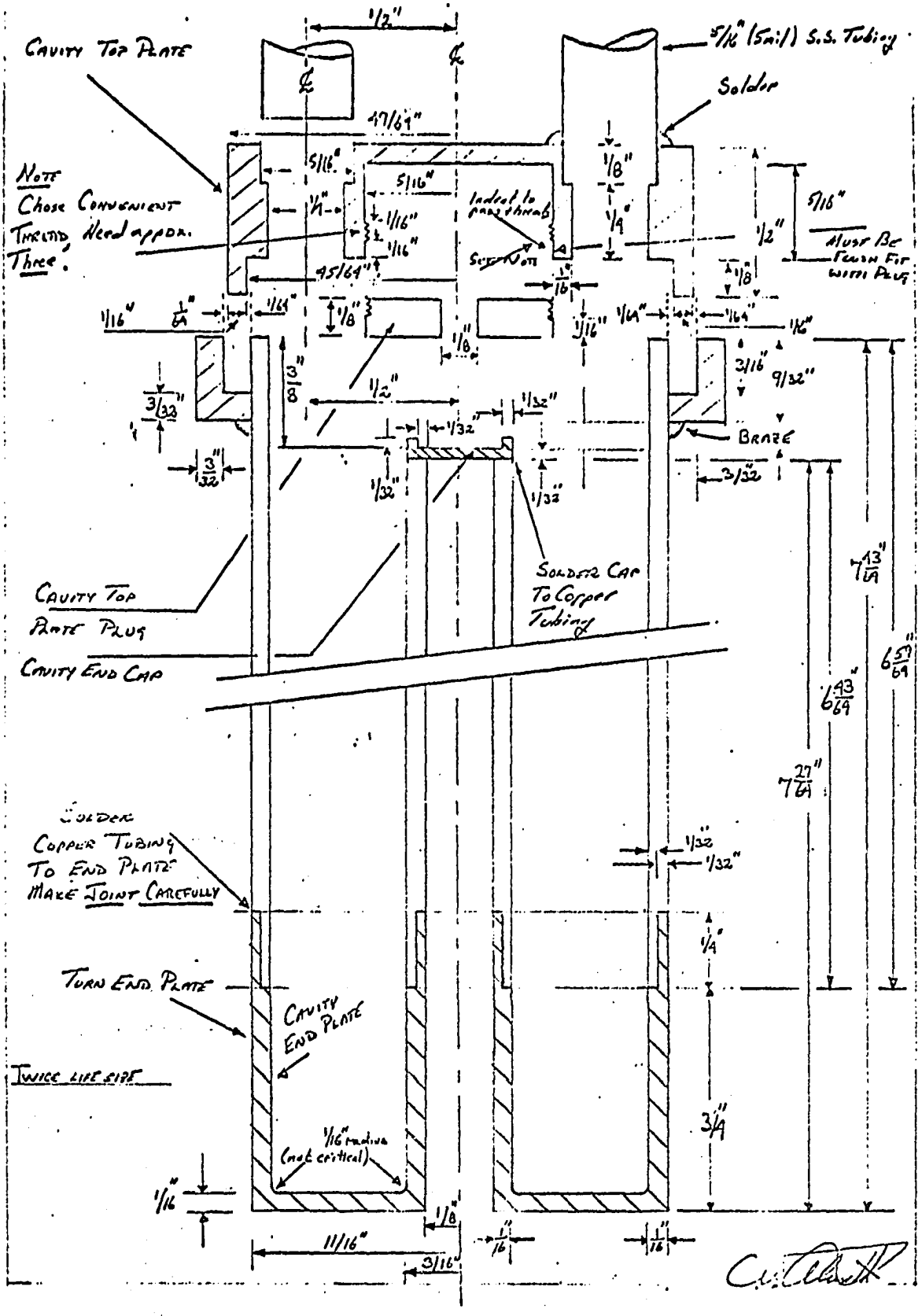

CAVITY – SIDE VIEW

Figure 4-4. Cavity Machine Drawing

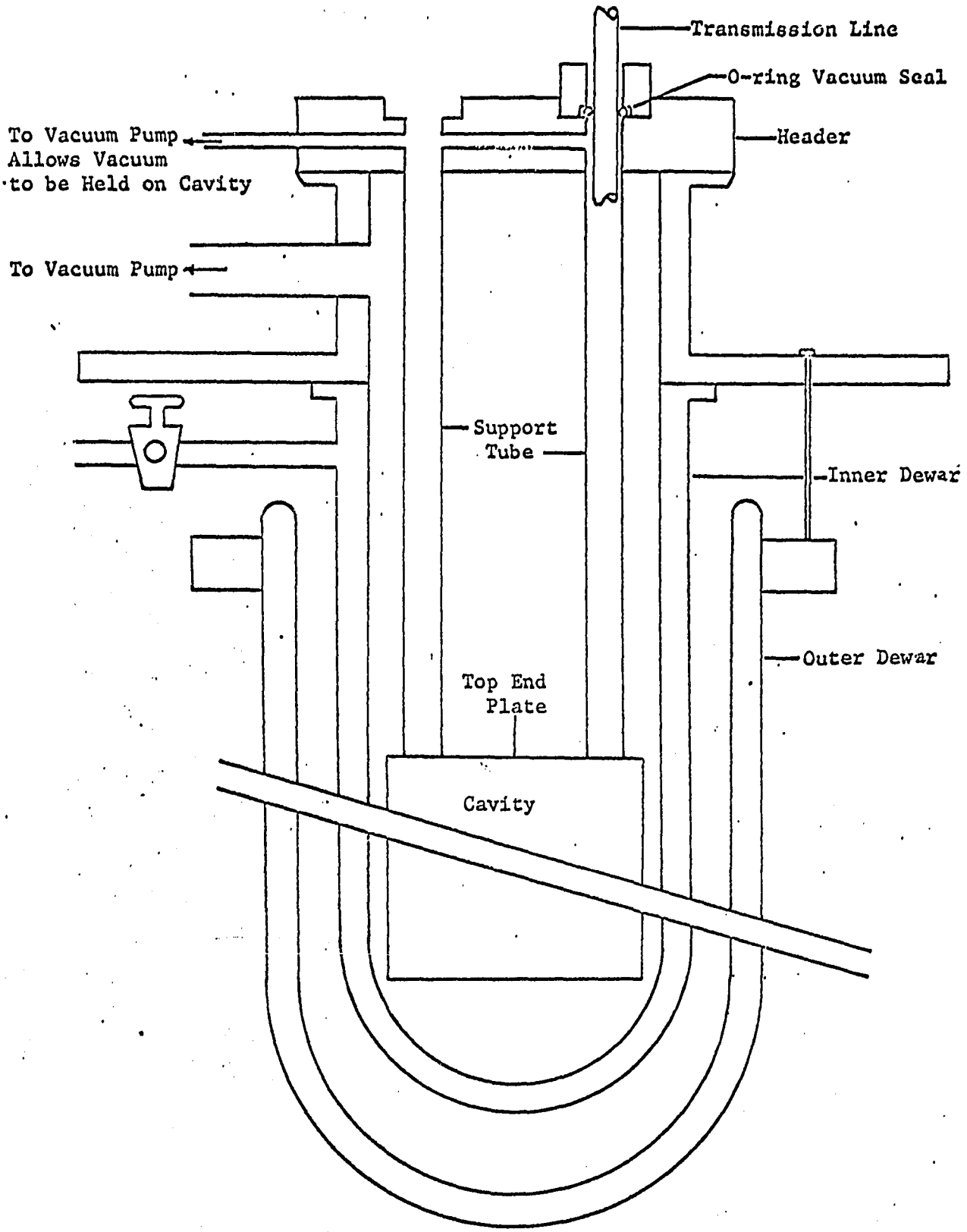

Figure 4-5. Cavity Cryogenic System

The header and stainless steel support tubes hold the cavity in the Dewar and allow a vacuum to be held on the cavity. Also the RF coaxial stainless steel transmission lines can run up and down inside the support tubes. Figure 4-5 shows the entire system inside the liquid helium Dewar.

Finally, the RF coaxial transmission lines had to be designed. Due to material limitations, the inner conductor was built of 1/8 inch ID stainless steel tubing and the outer conductor was 1/4 inch ID stainless steel tubing. The conductors were kept apart by seven 1/8 inch thick teflon spacers. Figure 4-6 shows a side view of the transmission line.

The impedance of a coaxial line is given by[20,35]

$$Z_o = \frac{Z_o'}{\sqrt{\left[1 + (\epsilon_r/\epsilon_o - 1)^{d}/_{s}\right]}} \qquad (4\text{-}1)$$

where d is the width of a spacer, s is the separation distance between spacers, ϵ_o is the dielectric constant of free space, and ϵ_r is the dielectric constant of the spacer. Z_o' is the characteristic impedance of the coaxial line if the only dielectric constant present were air, and Z_o' is given by[20,35]

$$Z_o' = 60 \ln D_1/D_2 \qquad (4\text{-}2)$$

where D_1 is the diameter of the outer conductor, and D_2 is the diameter of the inner conductor. Rearrangement of the equation (4-1)

yields

$$\left[\frac{Z_o'}{Z_o}\right]^2 = Z^2 = 1 + (\epsilon_r - 1)d/s \qquad (4\text{-}3)$$

where $\epsilon_r = \epsilon_1/\epsilon_0$, and thus

$$\frac{d}{s} = \frac{Z^2 - 1}{\epsilon_r - 1} \qquad (4\text{-}4)$$

The desired Z_o for the transmission line was 50 ohms, in order for good matching between the test equipment and the cavity. The value of Z_o' for a transmission line with $D_1 = 1/4$ inch and $D_2 = 1/8$ inch, was found to be 41.6 ohms. When these values of Z_o and Z_o' were substituted into equation (4-4), the value of d/s was given by

$$d/s = \frac{(0.694-1)}{\epsilon_r - 1} = \frac{0.306}{1-\epsilon_r} \qquad (4\text{-}5)$$

This meant that the desired value of 50 ohms was unavailable unless the values of D_1 and D_2 were changed. This was impossible due to long delivery times, and it was decided that the characteristic impedance of less than 50 ohms could be tolerated.

The relative dielectric constant of teflon spacers is approximately 2. Using this value of ϵ_r, and with d = 1/8 inch and s = 7 inches, Z_o is found to be 41.2 ohms.

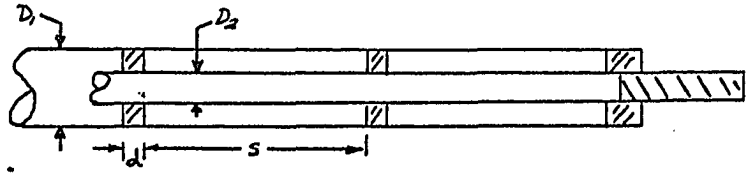

Figure 4-6. A Transmission Line

Stainless steel tubing was used because of its low coefficient of thermal conductivity. This was necessary because the cavity was at liquid helium temperatures, and heat losses had to be kept to a minimum. The low thermal conductivity coupled with a 5 mils wall thickness kept the heat loss low.

4.3 Preparation for Lead Plating

Since a high cavity quality factor is needed, and since the crystal exhibits its trap properties at 4.2°K, it was decided to lead plate the cavity. Lead becomes superconducting at about 7.2°K, and consequently the cavity would have a very high inherent quality factor. In order to obtain a good plate, certain rigorous procedures must be followed. These procedures will be explained in the following paragraphs. Additional information may be found in Boom and Hogaboom,[5] and in Rodgers.[41]

The plating solution used was the lead fluoborate form made according to the following formula.

Lead Fluoborate (50%)	800ml
Boric Acid Powder	144ml
Fluoboric Acid (50%)	266ml
Deionized Water	2570ml
Animal Glue dissolved in Distilled Water - Several Drops	

This formula prepared approximately one gallon of plating solution.

Several important precautions had to be taken. First, since the solution contained fluoboric acid, glass containers could not be used. Secondly, the boric acid powder was measured by volume, and finally the amount of animal glue used was vague. The rule of thumb in using animal glue was to add several drops to the plating solution, do some plating using the solution, and continuing to add animal glue until a slight darkening of the lead deposit was observed in high current density areas. This darkening is explained in Boom and Hogaboom, and will wash off after the plating is finished. The concentration of glue was not maintained, but when the plating deposits became rough, more glue was added.

The solution was prepared by dissolving the boric acid in deionized water. This step was done in an open glass container, since the boric acid powder dissolved slowly and had to be stirred. The boric acid was then transferred to a polyethylene container in which the plating solution was made up and kept. The lead fluoborate and fluoboric acid were then added. Reagent grade chemicals were used throughout, except for the lead fluoborate which was technical grade. Finally, the best quality animal glue and purest deionized water were used. The pH of the solution was kept at all times less than 1.5.

A perfectly clean part was absolutely essential if the plate was to adhere to the base metal and completely and evenly cover the metal. Two acid mixes, or dips, were used. A rough dip for cleaning, and a bright dip for polishing. These dips were prepared

according to the following formulae:

Rough Dip	Sulphuric Acid	73cc/128cc
	Nitric Acid	47cc/128cc
	Hydrochloric Acid	10cc/128cc
Bright Dip	Sulphuric Acid	73cc/128cc
	Nitric Acid	47cc/128cc
	NaCl	3.84gm/128cc

These solutions were always too fast (or too strong) and had to be diluted by placing a piece of scrap copper or brass in the dip until the solutions turned a murky green-blue. At this point, the scrap copper was removed, and the action of the dips was tested on a piece of brass. If the dips were still too fast, the scrap copper was returned to the dips, left for a few minutes, and then the dips were tested again. This was kept up until the dips operated as required.

When the dips became too weak, the solution took on the bright blue color of hydrous copper sulfate. When this occurred, more sulphuric acid was added until the solution turned a dark-dirty medium green. Approximate note was taken of the amount of sulphuric acid added, and approximately one half of this amount of nitric acid was added. At all times when the dip solutions were being used, or mixed, a chemical hood was used.

The procedure for cleaning a part for plating was as follows.

1. Rough Dip
2. Wash in tap water and then in pure water
3. Bright Dip

4. Wash in tap water and then in pure water
5. Diluted (1/2) Bright Dip
6. Wash in pure water
7. Put in the plating solution

The washing steps were extremely important in the preparation of the parts. First, all the dip had to be washed off in tap water; then all the tap water had to be washed off with deionized (pure) water. This had to be done fairly rapidly so that oxidization could not occur, particularly in the sixth step.

The lead anodes used in the plating process were made from high grade purity lead. The anode was then wrapped in mylar film and hammered into shape. Electrical contact was made by soldering a stiff copper wire into the anode. The copper wire and solder joint had to be covered with polyethylene tubing in order to avoid contaminating the lead plating solution. Finally, before the anodes were used, they were scrubbed with a clean tooth brush in a solution of Versene (Dow Chemical Cleaner).

4.4 Electroplating of the Cavity

Once the anodes, the plating solution, and the cavity parts had been prepared, they were ready for lead electroplating. In this process, the most important variable was the current density. If the density was too low, large grains would form, and if it was too high, treeing would result. Normally, the current density was maintained just below the treeing point.

The simple parts of the cavity were plated by pouring some plating solution into a polyethylene container, placing an anode in the solution and suspending the part, using copper wire in the solution. No contamination of the solution could occur since the parts and the wire were being plated. Furthermore, before the part was placed in the solution, a slight voltage was applied to the anode to reduce the chances of contamination of the plating solution. The parts were rotated occasionally.

The cavity end plate and the cavity were difficult to plate because of inside right angles and recesses. In order to plate the cavity, it was filled to the brim with plating solution, and an anode was placed inside the cavity and moved around until the plating was complete. In the case of the cavity top end plate, the transmission line holes were plugged with polyethylene plugs and the plating solution was poured into the end plate. An anode was then placed in the solution and moved around until the plating was complete.

Whenever treeing occurred, the tree was knocked loose by a polyethylene rod, or by first reducing the plating current and knocking the tree loose with the anode. The anode used to plate the cavity was semicircular in shape, whereas the anode used to plate the top plate was pencil-shaped with a blunt end.

A good deposit was considered to be the one with a satin

finish. The plating time used was approximately 20 minutes, more if needed or if trouble with tracing occurred, and the current had to be reduced. This would give a plate surface of approximately 0.010 to 0.020 inches. This was verified by weighing the part before and after plating. With the knowledge of the surface area and the density of lead, the value of plating thickness was determined. The thicker plate was desirable because the cleaning process removed considerable lead.

Once the desired amount of plating was obtained, the surface had to be dried and passivated. After the part was removed from the plating solution, or after pouring the solution out of the part, whichever the case may have been, the part was thoroughly washed in flowing deionized water. The part was then washed in Versene by allowing it to sit in the solution for 3 minutes. After this period of time, the part was again washed in flowing deionized water and placed in absolute ethyl alcohol for drying. Finally, the part was dipped in acetone and then dried by blowing dry nitrogen over it. The Versene solution was prepared according to the following formula:

Versene 100	140cc
Pure Water	7000cc
ME Dry Duponol	5gm

Several precautions had to be observed. First, the acetone had to be fresh and moisture free, and staining of the lead surface had to be kept to a minimum. If too much staining occurred, the part had to be washed in Versene long enough to remove the stain, then washed

in water, alcohol, and acetone, and dried, in order to entirely remove the stain.

Occasionally, it was necessary to completely strip the lead plate from the cavity. This was done by placing the part in a solution of acetic acid and hydrogen peroxide prepared according to the following formula:

80% Acetic Acid	100%
20% Hydrogen Peroxide	30%

If the part was to be replated, it had to be cleaned in the Bright Dip and the plating process restarted from the beginning.

Considerable care was taken when handling the lead plated parts, for natural oil from a person's hand would cause oxidization of the lead surface. However, it was known that the lead plate would stand the heat of soldering without visible degradation of the surface, so that joining the cavity together presented no problem.

4.5 Preparation of the Radioactive Source

The radioactive source chosen was carbon-14, which is a source of 156KeV betas. This source was prepared by evaporating a carbonate solution onto a polyethylene wafer, whose center had been hollowed out. The diameter of this wafer (or disc) was approximately 1 centimeter, so chosen because it had to fit in the recess of the cavity top end plate.

Several drops of the carbonated solution were placed in the hollowed section of the wafer, and the heat from a sun lamp was used to evaporate the solution. This process was repeated twice. In accordance with the wishes of the Health Physicist, the source was covered with a piece of cellophane paper. A sketch of the source is shown in Figure 4-7.

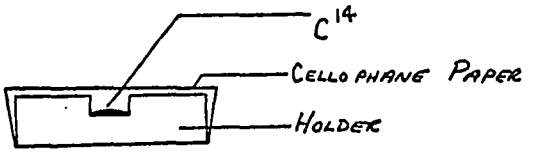

Figure 4-7. The Radioactive Source

4.6 The Effect of Cavity Geometry on Radiation Intensity

Radiation is emitted from a radioactive source in all directions. The fraction G of radiation which enters the window of a counter is a function of the radius r of the window and the distance h from the point source of radiation to the window. G, which is called the geometry factor, is equal to the ratio of the area S on the sphere enclosed by the window to the area of a whole sphere.[11] See Figure 4-8.

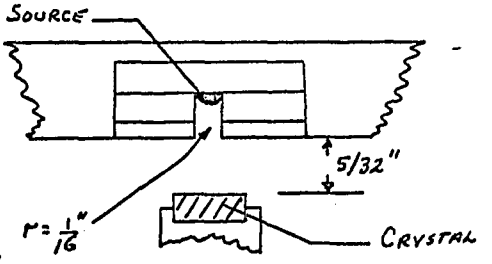

Figure 4-8. Counter Window

Therefore

$$G = \frac{S}{4\pi d^2} \tag{4-6}$$

the area enclosed by the window is given by

$$S = 2d^2(1-\cos\theta) \tag{4-7}$$

therefore G becomes

$$G = \frac{2\pi d^2(1-\cos\theta)}{4\pi d^2} = \frac{1-\cos\theta}{2} \tag{4-8}$$

or expressing $\cos\theta$ in terms of h and d

$$G = \frac{1}{2}\left[1-\frac{h}{d}\right] = \frac{1}{2}\left[1-\frac{h}{\sqrt{[h^2+r^2]}}\right] \tag{4-9}$$

Now the whole angle subtended by the window is

$$H = S/d^2 \tag{4-10}$$

and the area of the whole sphere is $A=4\pi d^2$, whereas the solid angle is $4\pi d^2/d^2 = 4\pi$ steradians. Thus the relationship between G and H becomes

$$G = H/4\pi \tag{4-11}$$

If the window is small compared to d and h, then d is approximately equal to h; therefore

$$G = \frac{\pi r^2}{4\pi d^2} = \frac{r^2}{4d^2} \tag{4-12}$$

For an enclosed proportional system, the geometry factor G is one half. For the cavity detector, the geometry factor will be different. Figure 4-9 shows the arrangement of the source to crystal, from which the geometry factor may be calculated. Note this calculation assumes a point source geometry.

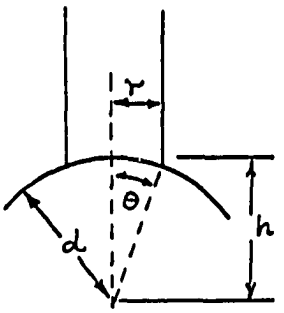

Figure 4-9. Cavity G Factor Diagram

Hence from Figure 4-9, r = 1/16 inch and d = h = 5/32 inch, and from equation (4-12), the G factor is 0.04.

This means that whereas a proportional counter can "see" 50% of the radiation, the cavity will only see 4% of the radiation actually present. Other effects, such as back scatter, will be ignored for now.

4.7 Preparation of the Cadmium Sulfide

The aluminum doped cadmium sulfide came from the supplier as an irregularly shaped crystal approximately 1.5 x 1.5 x 0.2 cm. From this piece, a crystal wafer 5/16 inch in diameter and 0.2cm thick was cut. A crystal of these dimensions would fit best on the re-entrant stub of the cavity. This wafer was cut from the supplied crystal, using an ultrasonic grinder and a special tool.

The special tool consisted of a piece of 5/16 inch ID copper tubing, one quarter of an inch long, soldered to the cutting head of the ultrasonic grinder. A preliminary cut was made on a glass microslide to see if the tool would work, and then the cut was made on the crystal.

No difficulty was experienced in cutting the crystal, but as the crystal was removed from the tool, part of an edge fell away. The crystal suffered only minor damage. In future crystal cutting, the method used by Hinds is recommended.[22] Hinds would cut his crystals part way and remove the cutting tool, then finish the cut with a sharp razor blade. This seems to be a good way of reducing edge damage to the soft cadmium sulfide crystal.

After the crystal had been cut, it was lapped with fine grade lapping compound on both sides. The crystal was then thoroughly cleaned, using deionized water, and allowed to dry. Finally, it was stored until needed. After the final wash, it was handled only with tweezers.

4.8 Determination of the Crystal Parameters

The impurity type was determined using the Seebeck effect. A piece of the irregular crystal was placed between two indium coated copper plates which were insulated from each other and which could be clamped tightly together. One of the copper plates was cooled by ice, and the other was heated, using a soldering gun. The potential difference between the two plates was due to thermal drift of the carriers in the crystal. This potential difference was measured using a Keithley 600A Electrometer. According to theory,[44] if the hot end is positive with respect to the cold end, then the crystal is N-type. If the hot end is negative, then the crystal is P-type. The crystal

was found to be P-type.

The crystal face was rotated 24° from the 001 plane towards the 102 plane, and the lattice spacing was normal. The aluminum doping was found to be 0.0264%. The literature showed that the trap level due to aluminum doping was 0.03eV below the conduction band.[12]

4.9 Reset Method

As mentioned in chapter two (2-7), there are four methods of resetting the crystal: heating to 200°K, infrared, tap effect, and electric fields. Because of the difficulty of placing an electric field of sufficient intensity in the cavity, or of obtaining infrared inside the cavity, only two methods of resetting the crystal were used: heat, and mechanical tapping.

Heat was applied to the crystal by placing a 24 ohm 2 watt wirebound resistor up the center of the hollow re-entrant stub. Voltage was applied to it whenever reset was required. This method proved to be successful, although it was not used very often since it caused undesirable boiling away of the liquid helium. The mechanical vibration proved to be easier and cheaper, since the crystal could be reset simply by banging on the header assembly.

The mechanical vibration method of resetting the crystal was unfortunate in some respects, because every time liquid helium or liquid nitrogen was added to the Dewars, the crystal was vibrated, thus causing partial reset. Further disadvantages were that no

clumsiness could be tolerated near the Dewar stand, for even a slight tap would partially reset the crystal.

CHAPTER V

EXPERIMENTAL TECHNIQUES AND INSTRUMENTATION

5.1 Introduction

Since several different techniques of instrumentation were used in conducting this experiment, and since in each case the cryogenic techniques were the same, this chapter will be divided into two parts. The first part will discuss the cryogenic techniques, and the second part will discuss the various techniques of instrumentation used.

5.2 Cryogenic Techniques

The assembled cavity was placed inside the Dewar system as shown in Figure 5-1. The inner Dewar was to contain liquid helium, and the outer Dewar liquid nitrogen. This arrangement of Dewars was used because liquid nitrogen is relatively inexpensive and boils at $77^{\circ}K$. The much more expensive liquid helium would only see a temperature gradient of $73^{\circ}K$, whereas the nitrogen would have a temperature gradient of approximately $233^{\circ}K$, depending on room temperature. The silver-coated evacuated Dewars would also serve to cut down on the heat loss to the system.

A mechanical pump was first used to evacuate the vacuum space between the walls of the inner Dewar through cock D. While this was

taking place, the stainless steel transmission lines were put in place and all vacuum seals were tightened. Next, the cavity and the inside section (A) of the inner Dewar were evacuated, using two mechanical pumps and openings C and B. These areas were then flushed with pure dry gaseous helium. The cavity and the inside section (A) were again exhausted and flushed with dry gaseous helium. This flushing of the cavity and inside section (A) of the Dewar was necessary in order to remove all signs of water vapor, otherwise water would condense and freeze inside the cavity, inside the stainless steel support lines - thus freezing the transmission lines in place - or on the inside walls of the Dewar, making it difficult to run the experiment.

Once the system was flushed, a slight positive pressure of helium gas was maintained on the cavity and inner section (A) of the Dewar assembly. Liquid nitrogen was then added to the outer Dewar. The liquid nitrogen was allowed to precool the inner Dewar and cavity for four to six hours. The latter period was preferred, but four hours was a minimum time period. The liquid nitrogen level was maintained as high as possible. The positive gaseous helium pressure was also maintained. During the first hour of the precooling period, the nitrogen level had to be "topped-off", or brought back to its preferred level, every twenty minutes. During the next hour, the nitrogen level had to be topped-off every thirty minutes, and during the final hours of the precooling time period, top-off was only necessary every hour. Each time the nitrogen was topped-off, the helium pressure

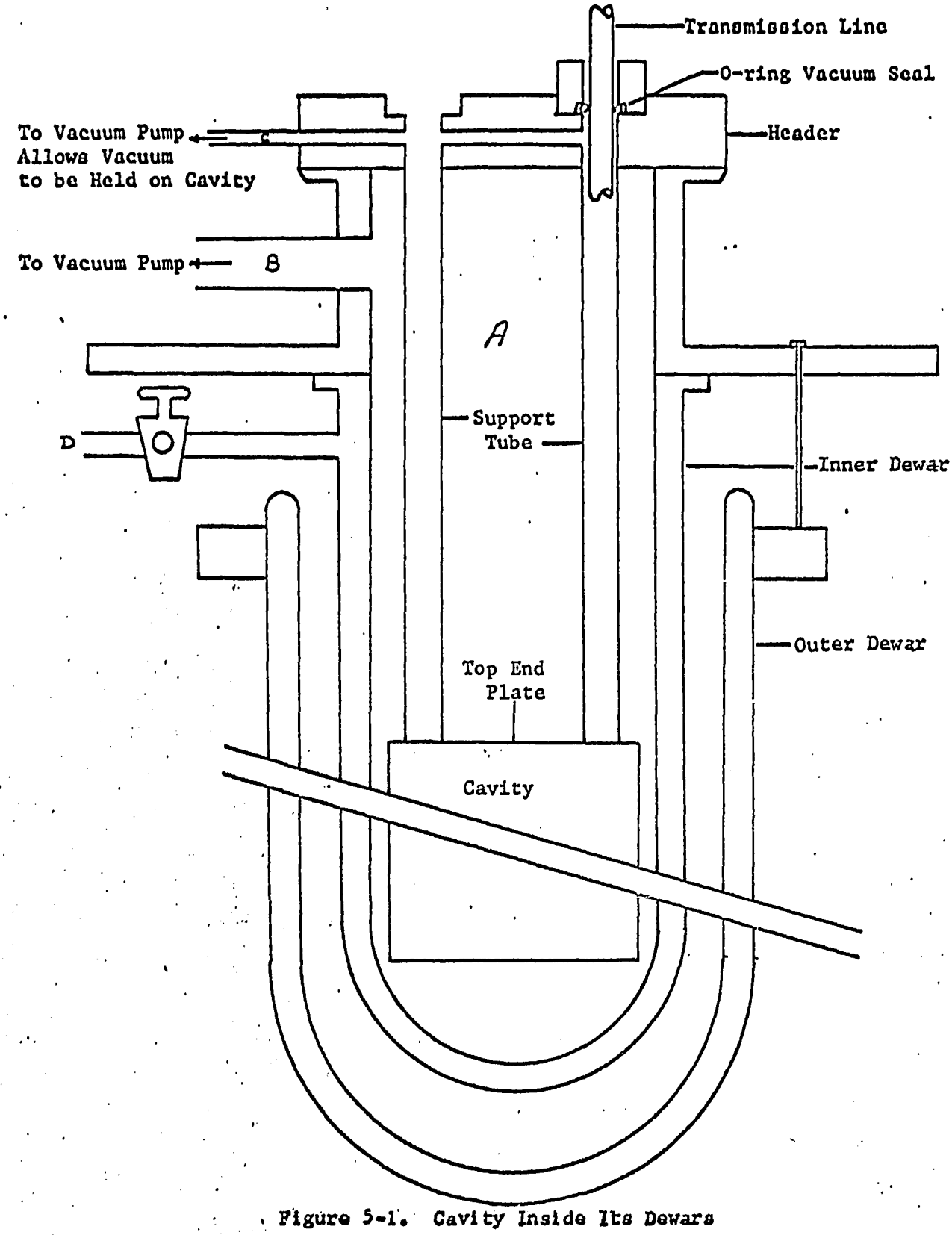

Figure 5-1. Cavity Inside Its Dewars

was checked and, if necessary, more helium was added to the system to maintain a positive pressure.

At the end of the precooling period, the liquid helium was transferred into the inner Dewar using a flexible liquid helium transfer tube which had been evacuated and flushed with dry helium before it was used. Liquid helium would begin to collect inside the inner Dewar after one minute if the longer precooling time had been used, or after three minutes if the shorter time period had been used.

The cavity was then allowed to stabilize for about fifteen minutes before it was considered to have reached thermal equilibrium. At this point, the experimental measurements described in the following sections could proceed. After experimental measurements were completed, the cavity was brought up to room temperature by allowing the liquid nitrogen and helium to boil off. Precautions were taken so that water vapor did not enter the system during warm-up.

5.3 Instrumentation Method Number I

A block diagram of the first method of instrumentation is shown in Figure 5-2 on page 85. This method was made necessary because the only frequency counter available was a 0-5 MHz counter. The cavity was driven by an HP 608E oscillator. Part of the output of this oscillator was mixed with the output of a phase locked HP 608F (Stability 2 parts in 10^7 sec) and the difference frequency

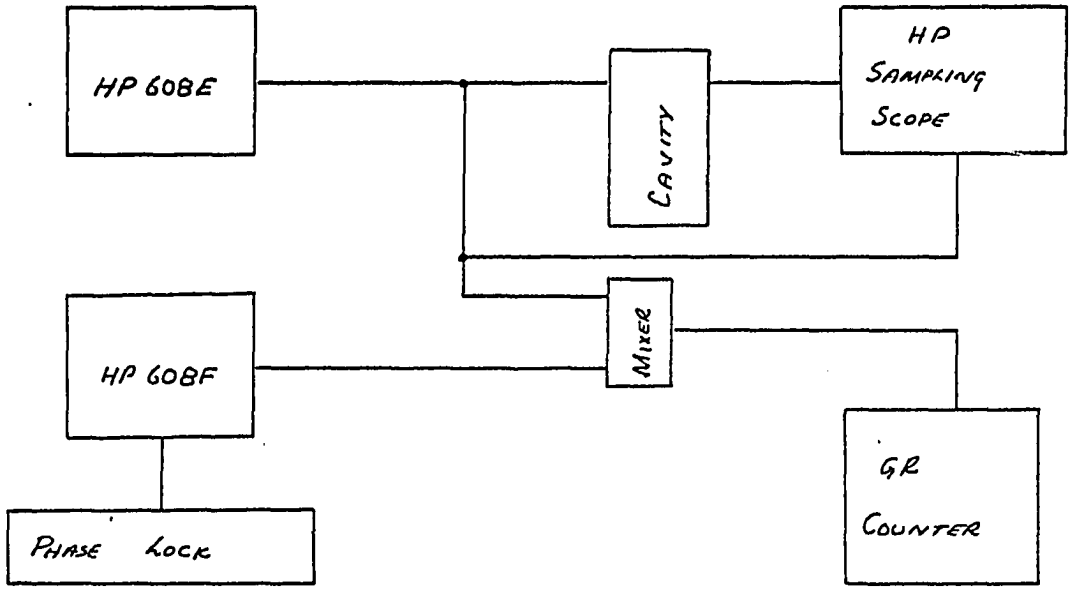

Figure 5-2. Instrumentation System Number I

was applied to the G.R.counter. The output frequency of the HP 608E was then varied until it was exactly at the resonant frequency of the cavity. This was accomplished by adjusting the frequency of the HP 608E until a maximum was noted on the scope. This oscillator was then peaked every ten minutes and the reading of the G.R.counter (the difference frequency of the 608F and 608E) was recorded. The operating frequency of the 608F oscillator was also recorded.

5.4 Instrumentation Method Number 2

A block diagram of the second instrumentation system used appears on page 86 in Figure 5-3. This method was used because the HP 608E was unavailable at the time, and also because it was hoped

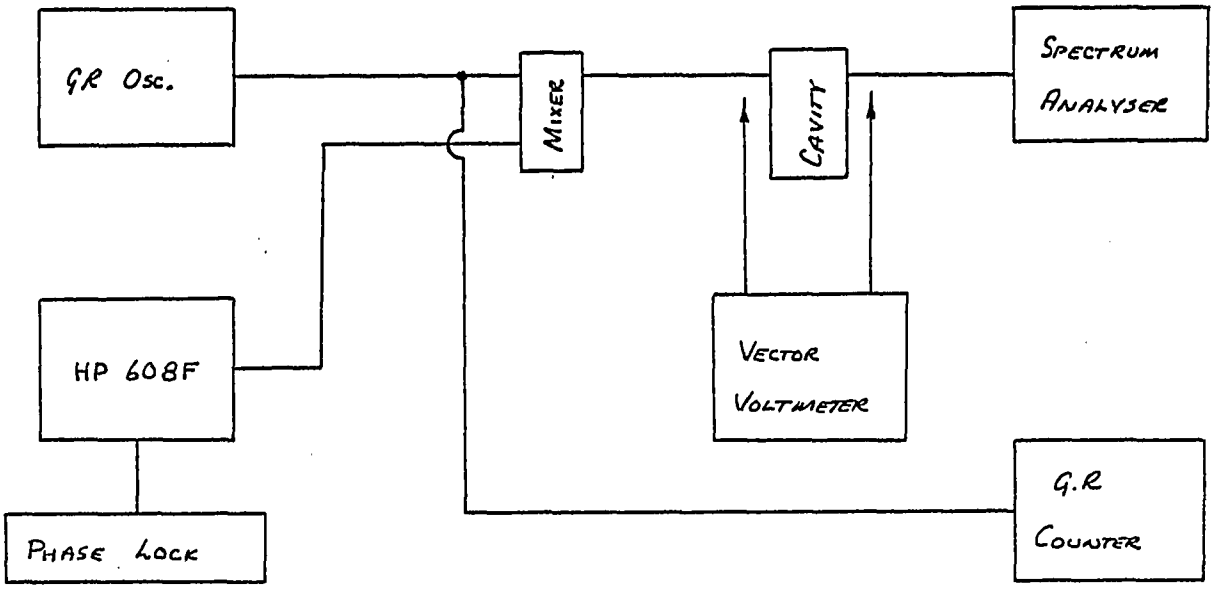

Figure 5-3. Instrumentation System Number 2

that easier adjustment of the cavity driving force would be possible. The primary advantage was that the G.R.oscillator generated at lower frequencies, which could be counted with the 5 MHz counter. The output of the G.R.oscillator and the HP 608F were mixed and applied to the cavity. The frequency of the HP 608F and the G.R.oscillator were so chosen that the difference frequency was the resonant frequency of the cavity. As the frequency of the cavity varied due to radiation, the frequency of the G.R.oscillator was varied. The adjustment of the G.R.oscillator was made so that the output seen on the spectrum analyser was maximized. The vector voltmeter was used to obtain 40 db of decoupling.

The HP vector voltmeter has two input channels, A and B, with which it is possible to measure voltage ditferences. Channel A

was placed on the input side of the cavity and channel B was placed on the output side of the cavity. The cavity was then lightly coupled, and the voltage difference between the input and output terminals was noted. The input and output transmission lines were then adjusted so that an additional 40 db difference in voltage between the two terminals was obtained. The input transmission line was adjusted to obtain 20 db difference, then the output line was adjusted to obtain the total of 40 db.

5.5 Instrumentation Method Number 3

A block diagram of the third method of instrumentation is shown in Figure 5-4, below.

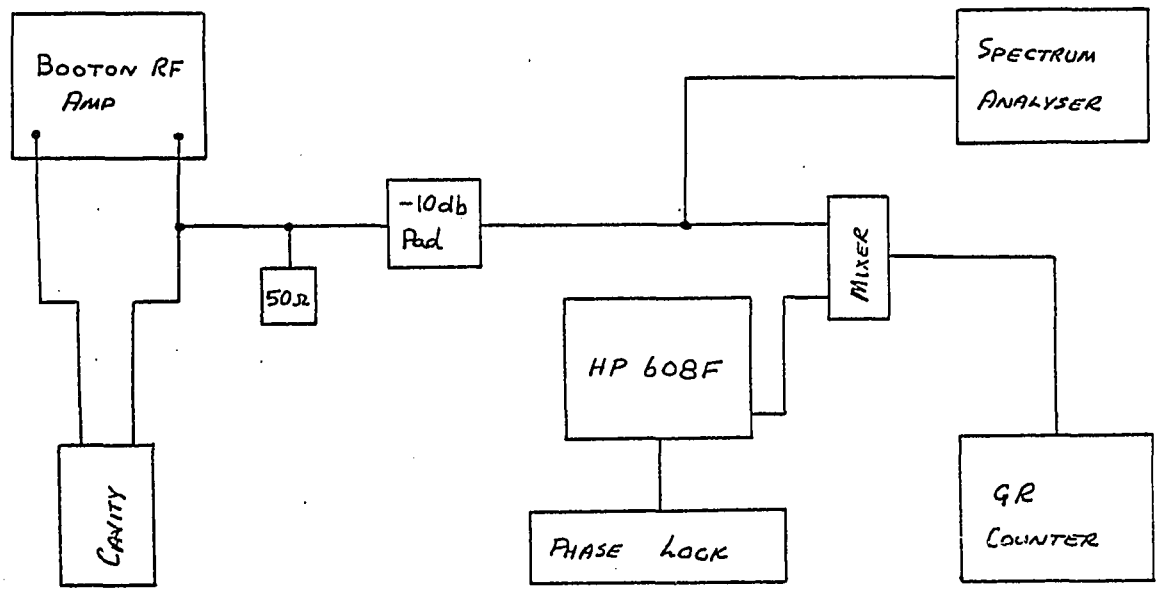

Figure 5-4. Instrumentation System Number 3

In this case, the cavity was used as the feedback element in an

oscillating closed-loop system. The output frequency of the cavity was mixed with the output of the phase-locked HP 608F, and the difference frequency was measured by the G.R.counter. As the resonant frequency of the cavity changed, the band width of the RF amplifier had to be peaked, and the new oscillation frequency measured. The real drawback to this system was the large amount of RF energy dissipated in the cavity, which caused the liquid helium to boil off at a very fast rate.

5-6 Instrumentation Method Number 4

A block diagram of the fourth method of instrumentation is shown in Figure 5-5, below.

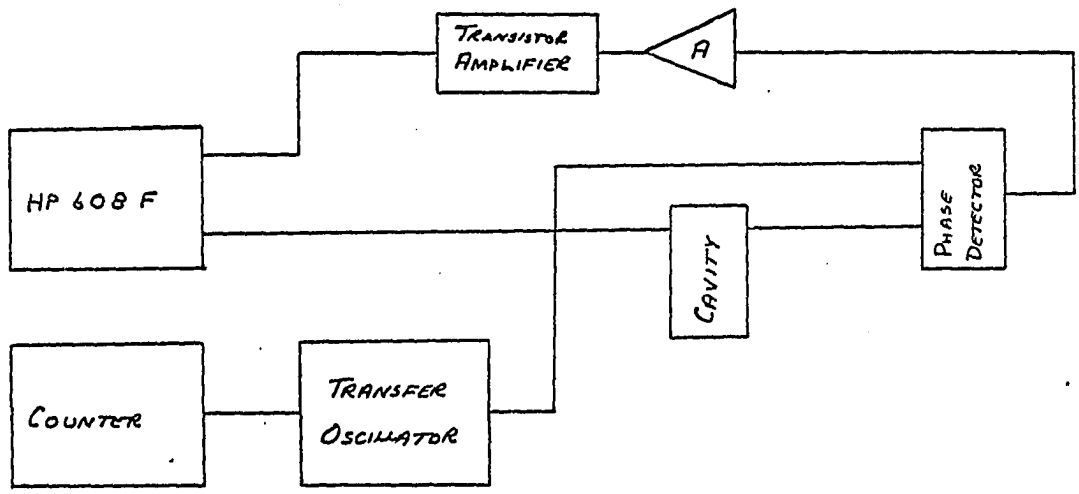

Figure 5-5. Instrumentation System Number 4

In this system, the HP 608F was phase-locked to the cavity and its signal was allowed to change as the cavity resonant frequency changed. This system takes advantage of the sharp change in phase of a signal

about the resonant frequency. The frequency of the system was measured directly, using a transfer oscillator and a counter. As the cavity resonant frequency changed, the phase relationship between the input signal to the cavity and the output signal of the cavity would also change. This change was sensed in the mixer which was now operating as a phase detector. The change thus appeared as a DC voltage.

The DC voltage was amplified in an operational amplifier, and the output voltage was directly coupled to a transistor amplifier which drove the HP 608F. The transistor amplifier was so designed as to drive the HP 608F, which responded to voltage changes from 0 to -50 volts (DC) with a 4K input impedance. Thus when the cavity and HP 608F were operating at the same frequency and there was no phase error in the signals, the transistor amplifier would put out -15 volts. As the frequency of oscillation changed, it was recorded.

This system of measurement was by far the most superior, since it responded to a change in phase. The change in phase was much easier to observe than the corresponding change in amplitude. Secondly, the system itself would automatically follow the changing resonant frequency, thus reducing the chance of experimental error, as reflected in a reduction of the scatter of the data.

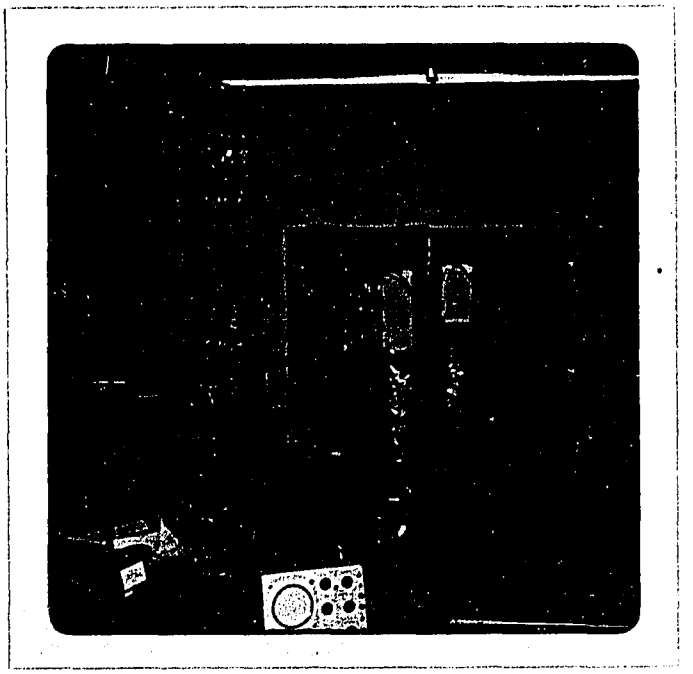

Plate I. General View of Experimental Apparatus
Note electronic equipment is on the left, and the cavity in its dewar stand is on the right.

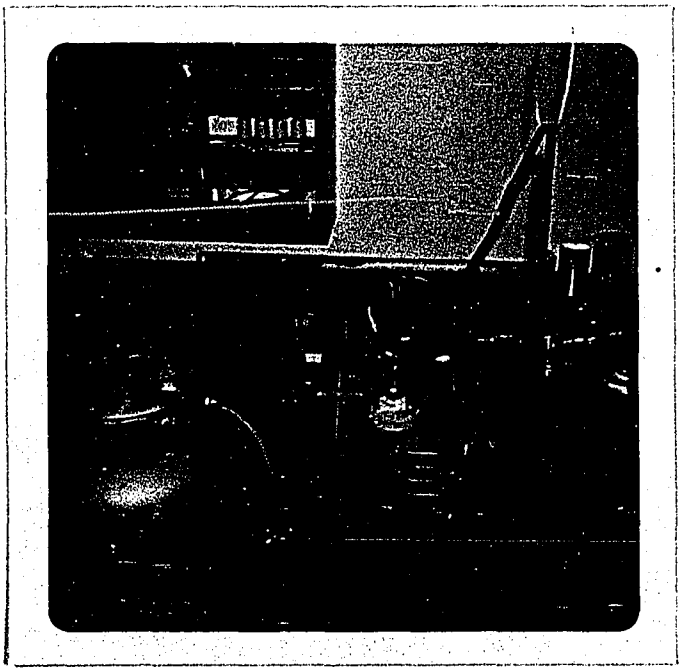

Plate II. View of the Cavity Header
The white ring at the top of the outer dewar is frost caused by water condensing due to the extreme cold of the nitogen gas.

CHAPTER VI

RESULTS, CONCLUSIONS, AND RECOMMENDATIONS

6.1 Results

The results of the experiments are shown in figures 6-1 a and b, 6-2 a and b, 6-3, and 6-4 a and b. The data of figure 6-1 were taken on the experimental run making use of the first instrumentation method. The data of figure 6-2 were taken some time later using the second method of instrumentation. That of figure 6-3 were taken using the third method. Note that in this particular experimental run, the liquid helium boiled off very quickly, as explained in section 5-5, allowing only one set of data to be taken. Finally, the results shown in figure 6-4 were taken using the fourth instrumentation method.

It should be obvious immediately that none of the slopes is the same in the four figures. This is unfortunate, because the results should be repeatable; however, the reasons that the data is not repeatable are simple. Between each of the experimental runs used to record data, the cavity was opened, the lead plate checked and then resealed. Each time the cavity was opened and resealed, the Woods metal seal had to be heated, with the result that the radioactive source was heated also. The radioactive carbon 14 source was in the chemical form of a

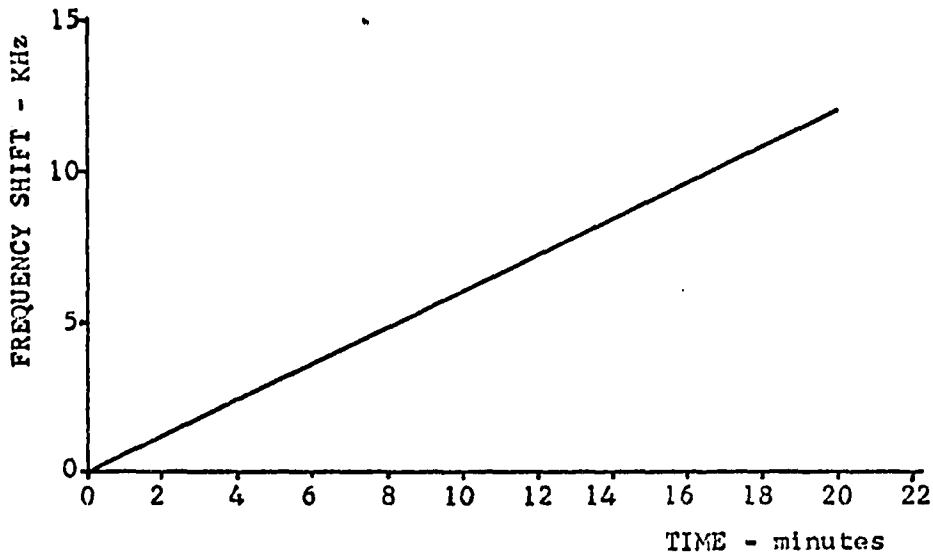

Figure 6-1a. Results of Run Number 1

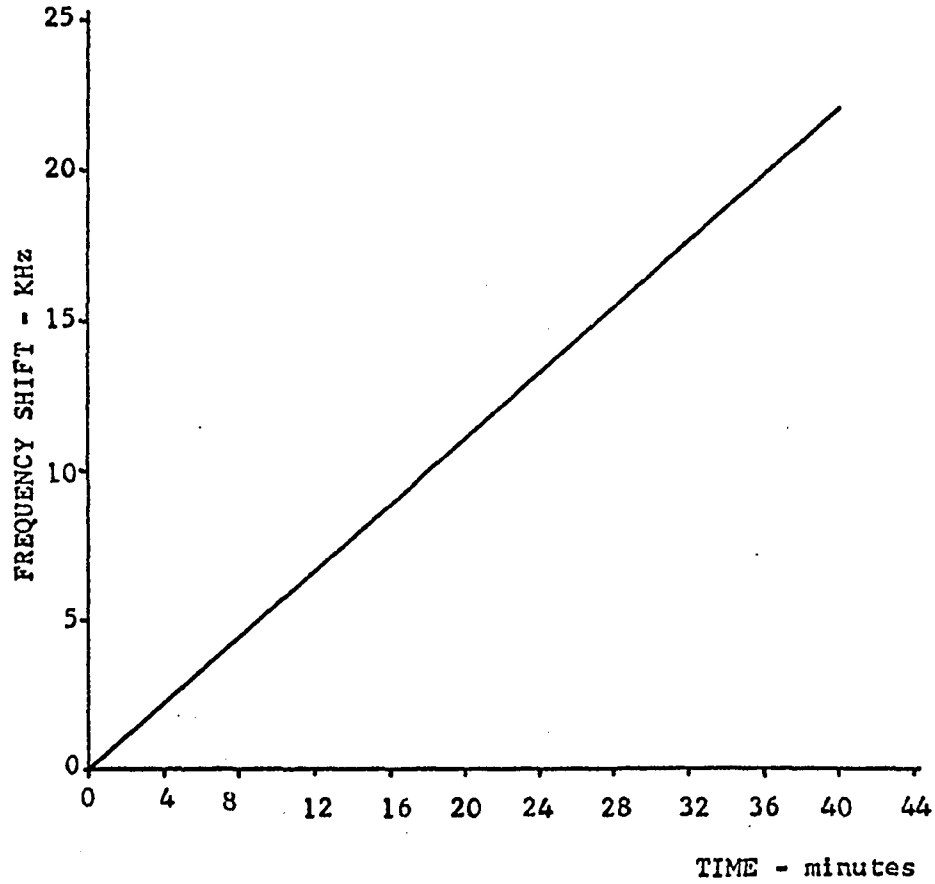

Figure 6-1b. Results of Run Number 2

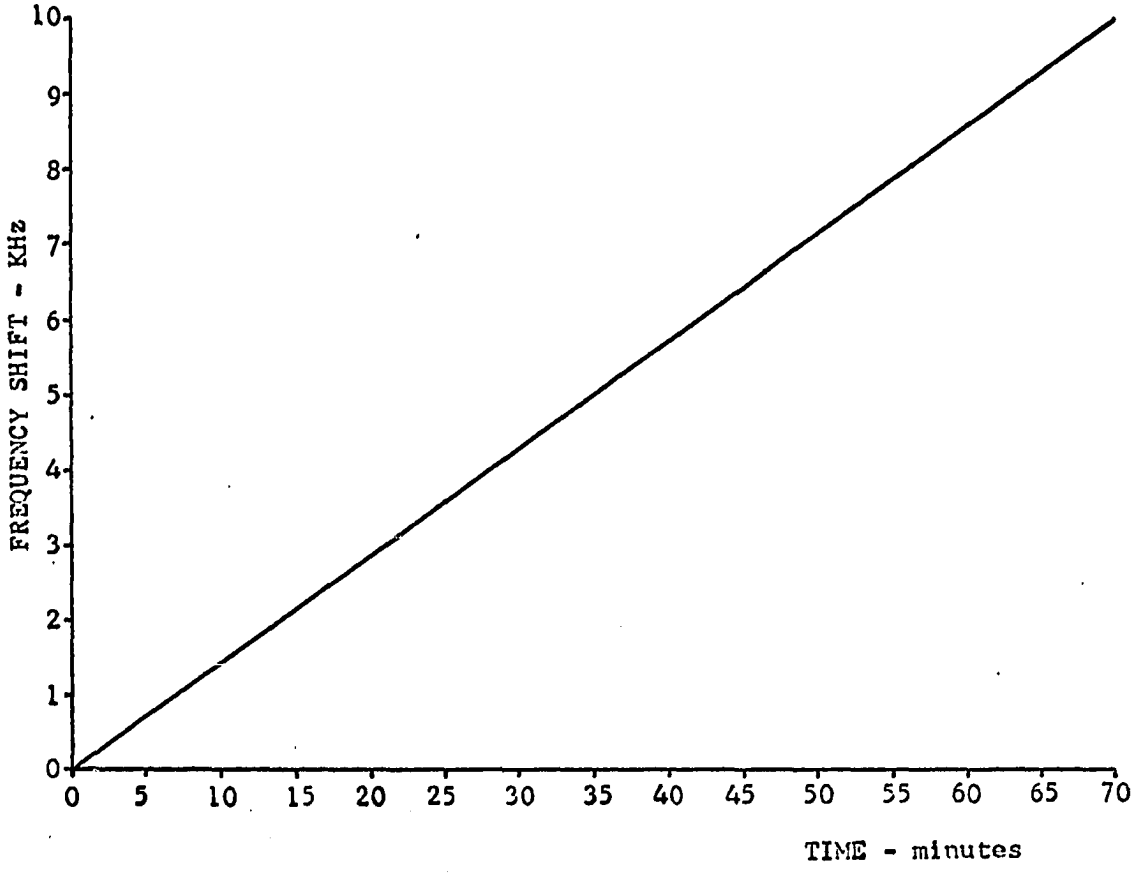

Figure 6-2a. Results of Run Number 3

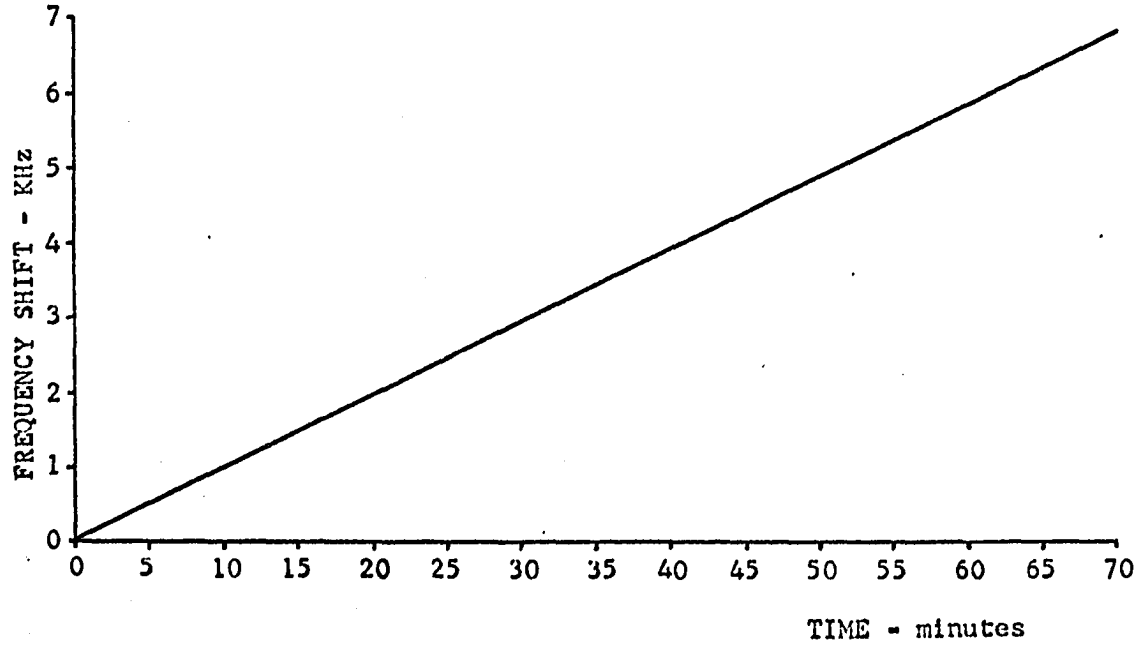

Figure 6-2b. Results of Run Number 4

carbonate, and the heat caused the source to decompose chemically into an oxide and carbon dioxide. The result of the chemical decomposition was to reduce the overall radioactivity of the source.

Figure 6-5 shows the radiation characteristic of the source just after it was prepared. The data were taken in a gas proportional system. Figure 6-6 shows the radiation characteristic after the source had been heated four times (that is, the cavity had been opened and resealed twice.) The data were taken in the same proportional system.

The cavity and source were heated first when the cavity was sealed for the first run. Very little heat was used because the Woods metal set up very nicely in a fresh joint. The data for experimental runs 1 and 2 were then taken. The equipment was later readjusted to take experimental run 3; however, the cadmium sulfide crystal was jarred off the re-entrant stub. (This is reported in section 6-2.) The cavity had to be opened in order to replace the semiconductor crystal. The first time the cavity was opened, considerable difficulty was encountered and the cavity was intensely heated. The second time the cavity was sealed, intense heating was needed in order to get the cavity top plate to set down inside the well (see figure 4-3.) Therefore, between runs 1 and 2, and runs 3 and 4, the cavity was intensely heated twice. The second time the cavity was opened, very little heat was used due to experience gained during the preceding opening and sealing operations.

The intensity of the source, as measured by a gas proportional system on the beta plateau, dropped from 16,200 cpm (counts per minute)

to 4,500 cpm after being heated. Now recall the explanation regarding heating offered in the preceding paragraph, and assume the source to be at almost full strength for runs 1 and 2, ie., 16,200 cpm, and at minimum strength, ie., 4,500 cpm, for runs 3 and 4. This means that the intensity had dropped by 72%. The slope of the frequency shift for runs 1 and 2 is 620 Hz/min, and the slope for runs 3 and 4 is 130 Hz/min, or a change of 79%; this shows fairly close correlation between the data and the results. The assumptions on how heating affects the source are somewhat gross, since there is no way to know exactly how much heat was applied. The data does show, however, that as the radiation flux falls off, so does the change in frequency. Even without these assumptions, the frequency shift is related to the radiation flux as predicted. (The linearity of the shift can only be surmised, although the theory shows that the shift should be linear.)

The additional difference between the two runs can be accounted for by the fact that the cavity top end plate could not be placed as near to the re-entrant stub for runs 3 and 4 as for runs 1 and 2 because the Woods metal would not permit the plate to pull in place completely in the well (as explained previously.) This would change distance B (see figure 4-2), which in turn changed the electrical properties of the cavity. This explained in the next paragraph.

It should be pointed out that there are two geometry factors involved in the cavity. One is the nuclear radiation (G) geometry factor, as explained in section 4.6; and the other is the electromagnetic (K) geometry factor, as defined in equation (3-58). Any change, however minor, in the dimensions of the cavity will alter the K factor. The

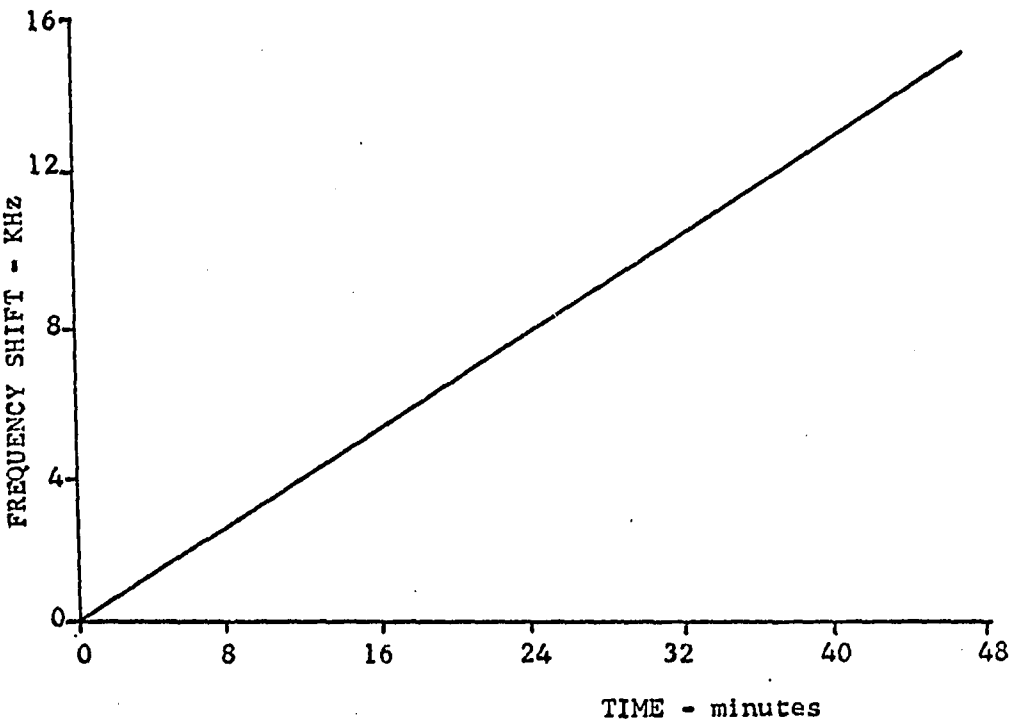

Figure 6-3. Results of Run Number 5

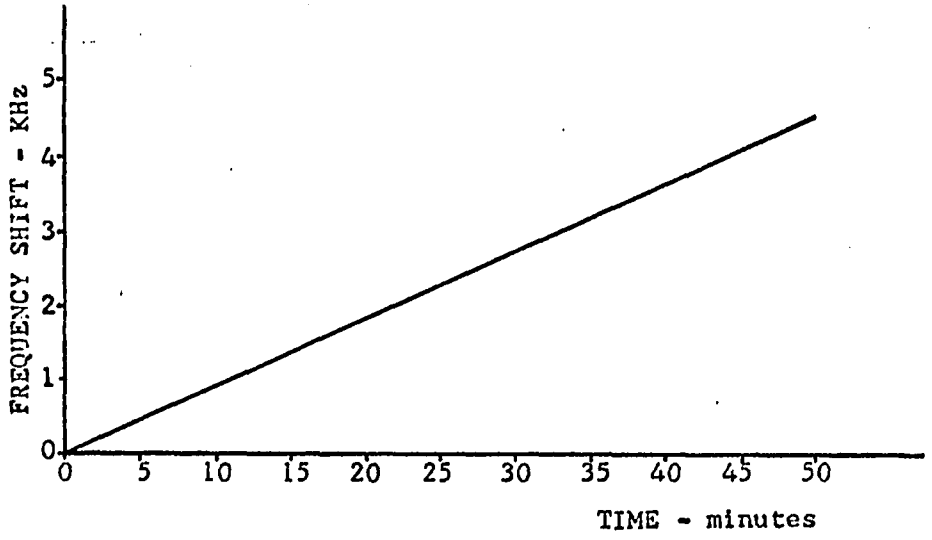

Figure 6-4a. Results of Run Number 6

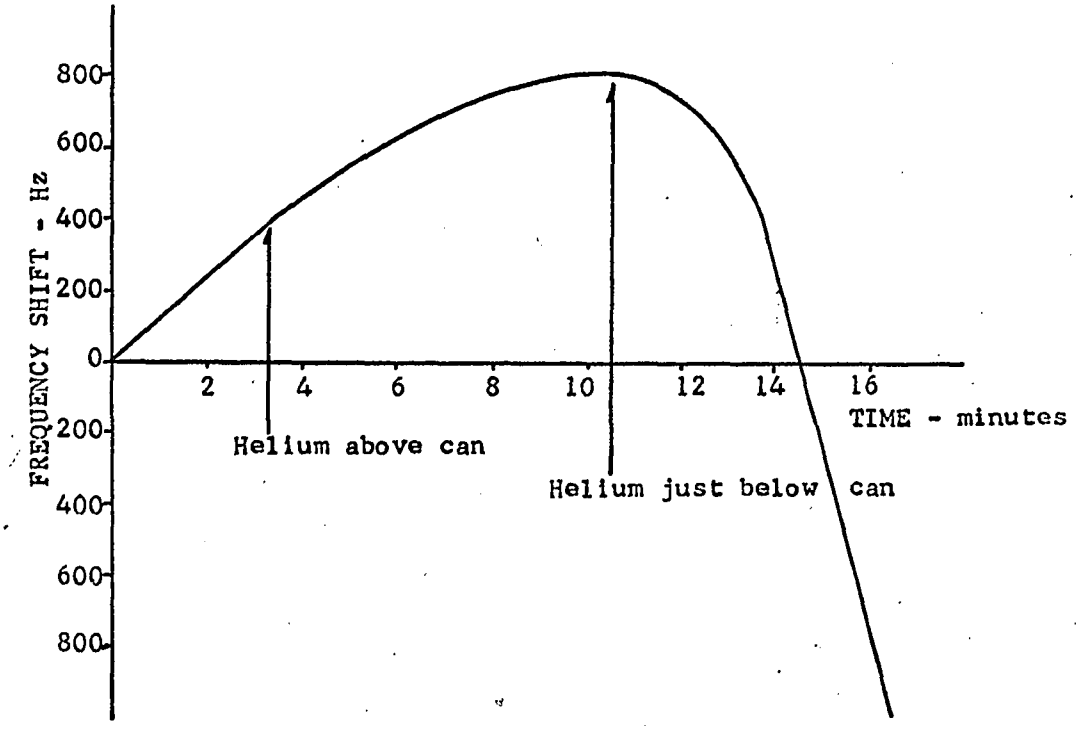

Figure 6-4b. Results of Run Number 7, Showing the effect of loss of Helium on the results. Note how the system follows the decreasing frequency.

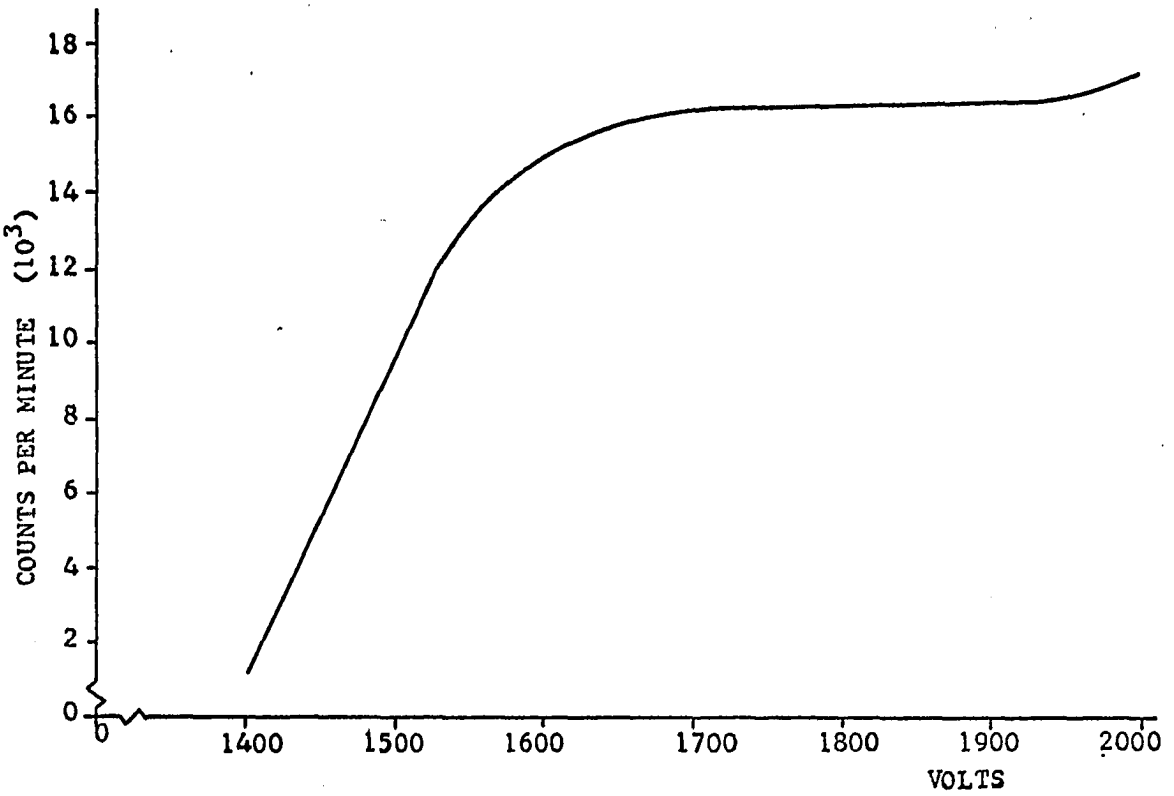

Figure 6-5. Initial Characteristic of Source

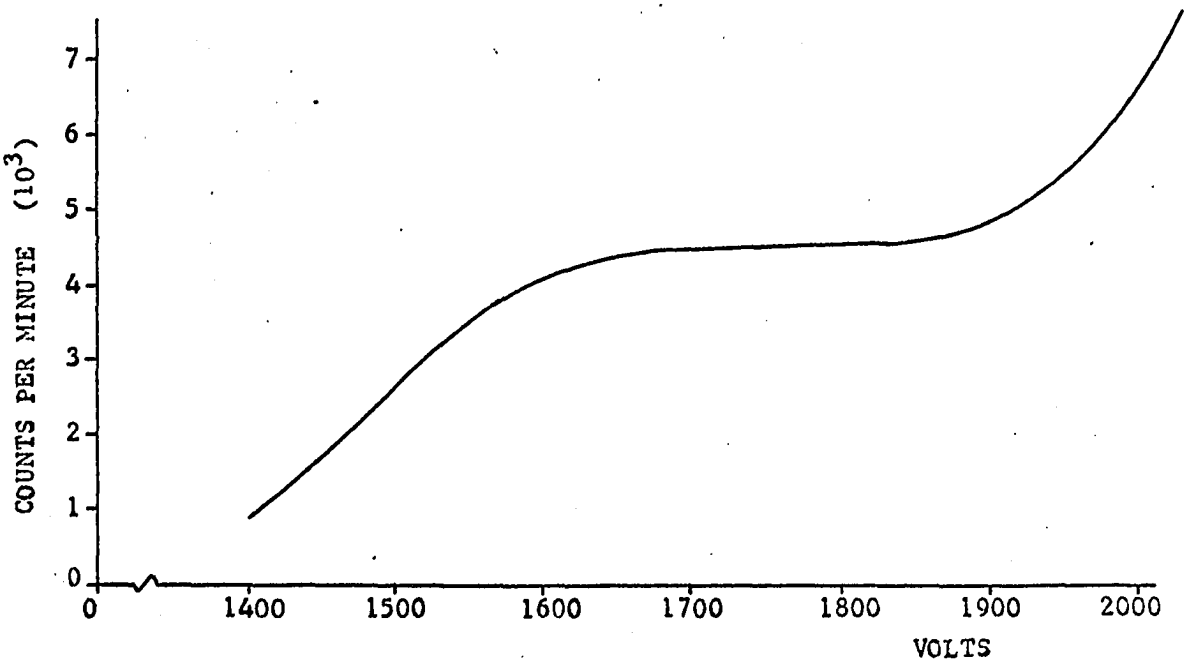

Figure 6-6. Characteristics of Source after Heating

G factor relates the amount of radiation given out by the source to the amount of radiation seen by the crystal, or dosimeter. In the case of a gas proportional counter, this factor may be as high as 50%; in the case of the cavity the factor is 4% (see section 4.6) for a point source geometry.

Between the fourth and fifth data runs, the cavity was foreshortened by placing a one-eighth inch metal plate between the re-entrant stub and the top end plate (see figure 6-7).

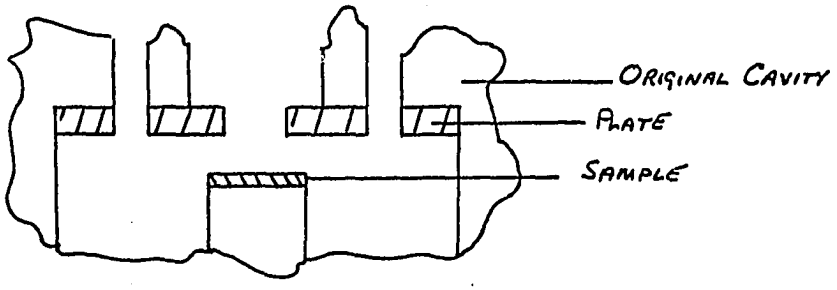

Figure 6-7. Foreshortened Cavity

By shortening the cavity, the effect of a change in crystal dielectric constant would be greater on the resonant frequency. This means that the third set of data was taken with a different cavity geometry, and since the cavity was heated, a further reduced radioactive source. The addition of this plate would possibly reduce the source geometry. In this case the slope was 321 Hz/min.

Each of the curves shows a shift in frequency which is approximately proportional to the intensity of radiation. That is, a slope of 620 Hz/min corresponds to a count of 16,200 cpm in a gas proportional

system. A slope of 130 Hz/min corresponds to a count of 4,500 cpm in a gas proportional system. Notice that with the change in cavity geometry (K) and possible change in source geometry (G), and assuming that the heat did not appreciably change the intensity of the source, then a slope of 321 Hz/min also corresponds to 4,500 cpm (see figure 6-3).

6.2 Other Runs

One run was made during the experimental work in which no frequency change was recorded. This was somewhat shocking to the experimenter. Data taken during this run showed that the operating frequency would change if the cavity were heated, but that after five minutes the resonant frequency returned to its preheated value. (Heating was accomplished through a 24 ohm-2 watt resistor inserted inside the hollow re-entrant stub.) The system was hammered on with no change in frequency resulting. The cavity factor Q was measured and found to be $(2.3)(10^5)$. Normal Q measurement was $(3.00)(10^4)$. This lead the experimenter to suspect that the crystal was no longer on the end of the re-entrant stub.

After the experimental run, the system was brought back up to room temperature, and the cavity was carefully opened so as not to jar the crystal off the re-entrant stub. The crystal was not in place, but was found in the bottom of the cavity where it would least affect the operating frequency. The result of this run was to show that any previously recorded cavity resonant frequency changes are due to radiation striking the crystal, since there was no change when the crystal was not in place.

6.3 Conclusions

The purpose of this dissertation was to prove that the photodielectric effect could be used to detect nuclear radiation as a dosimeter, and this has been done. The theory developed shows that the change in frequency is predicted by

$$\frac{\Delta f}{f_1} = \frac{\Delta \epsilon_r'}{\epsilon_r^2} K \qquad (6\text{-}1)$$

which is a combination of equations (3-54) and (3-62). The change in $\Delta \epsilon_r'$ is given by equation (3-42), and the change in Δn is given by equation (3-39). A combination of these two equations yields

$$\frac{\Delta f}{f_1} = \frac{K}{(w_o^2 - w^2)} \frac{e^2}{m e_o \epsilon_r^2 V} \alpha \int_0 \phi(t)dt \qquad (6\text{-}2)$$

but w^2 is small compared to w_o^2, as shown in chapter three; thus

$$\Delta f = \frac{f_1 K e^2}{w_o^2 m e_o \epsilon_r^2 V} \int_0^t \phi(t)dt \, . \qquad (6\text{-}3)$$

All the terms in the above equation, with the exception of the integral, are constants, thus

$$\Delta f = \overline{K} \int_0^t \phi(t)dt \, . \qquad (6\text{-}4)$$

In the case of the experimental runs undertaken $\phi(t)$ was a constant, thus

$$\Delta f = \overline{K} \phi t \qquad (6\text{-}5)$$

which is linearly related to time.

The results obtained in the experimental runs are linearly related to time. Also as ϕ decreased, so did the slope of the results. Thus the cumulative photodielectric device behaves as predicted in the theoretical development, and the effect may be used as a radiation dosimeter. Also, according to the theory developed, the dosimeter should work with very low

activity, low energy sources. This would extend to energies well below the 156 KeV (maximum) used for the experiment, and possibly to 2.54 eV, the bandgap of cadmium sulfide.

6.4 Advantages of This Technique

Because the device is an integrator, and since all the ionized holes and electrons are trapped, it becomes very sensitive to low energies and low flux. That is, only about 5 eV is required to ionize an electron-hole pair in CdS. These are trapped and in effect "counted". Thus every pair created in the crystal by ionizing radiation is significant, and very low intensities may be observed. Since recombination does not occur (for days), no recombination noise is present in the semiconductor crystal. No shot or flicker noise exists, since there is no current flowing in the crystal. The only other appreciable noise source which would mask the 5 eV sensitivity figure is that generated by thermally excited hole-electron pairs which might fill the traps. This may be discounted by considering the relationship for conduction electron density (n_i) in a semiconductor given by equation (6-6).[38]

$$n_i = \frac{4\sqrt{2}}{h^3} (\pi m_e k T)^{3/2} e^{-Eg/2kT} \qquad (6\text{-}6)$$

where h is Plank's constant, k is Boltzman's constant, Eg is the energy gap in cadmium sulfide, and T is the temperature in degrees Kelvin. At room temperature ($300^{\circ}K$), Eg equals 2.53 eV, and k equals 0.026 eV. The use of these numbers in equation (6-6) yields an intrinsic density of conduction electrons of $(1.42)(10^3)/m^3$. In a sample having a volume of 0.1cc, only $(1.42)(10^{-4})$ electrons would exist, on a time average. The creation of a single hole-electron pair would be three orders of

magnitude above this noise. At lower temperatures this noise figure would be even lower.

A further improvement in the noise characteristic of the device arises because frequency is measured rather than an amplitude. The system does not require that the dosimeter be separated from the radiation source by an intervening wall.

In summary, the cumulative photodielectric effect (AC mode) dosimeter offers several worthy advantages. These include a reliable built-in integration effect (that is, no external electronic circuits are required to register the rate of dose), high sensitivity to low energies (of the order 5 eV, the ionization potential of cadmium sulfide), low flux capability, low device noise, and improved electronic circuit noise figures.

6.5 Discussion

At the start of the experimental work, the primary goal was to show that the photodielectric effect in cadmium sulfide could be used as a nuclear radiation dosimeter. This goal was accomplished. It was also hoped that several sets of data runs could be made using three different sources of radiation (alpha, beta, and gamma.) Also a series of data runs was to be attempted using high purity silicon (10K/cm) in place of the cadmium sulfide crystal. Finally, the dosimeter was to be calibrated using a known source of radiation.

All of these goals were impossible to attain, not because of improper experimental objectives, but because local funding was not

available for the purchase of enough liquid nitrogen and helium. The primary goal of proving the feasibility of the device was achieved. It is hoped that the preliminary data obtained to date may be used to convince some agency that the cumulative photodielectric effect may be used as a means of nuclear radiation dosimetry. If this can be done, further sets of data can be obtained.

6.6 Recommendations For Further Study

The cumulative photodielectric effect has been shown to be useful in the construction of a dosimeter, but no calibration run was made with this device. One of the first steps that should be taken is calibration of the device, so that it may be used to measure unknown quantities of radiation. Furthermore, the effect should be studied for various types and intensities of radiation; for if the device is to be used as a dosimeter, it must be able to measure an amount of energy deposited per unit time from any radiation source. The dosimeter should have a response to the energy deposited which is essentially independent of the energy and of the nature of the radiation.

Other crystals should be investigated to see if they exhibit cumulative traps at higher temperatures. This should be possible, since the literature[30] indicates that CdS:Ag exhibits the trap property up to $70^{\circ}K$. This is unfortunate since the temperature of liquid nitrogen is $77^{\circ}K$; but if different dopants are tried it may be possible to sustain these traps inside temperature range of liquid nitrogen. Even at the temperature of liquid nitrogen, the system would be difficult to use. It is hoped that a method could be derived for which the device would

operate at room temperature.

Some mention of the source geometry factor was made in section 4.6, for a point source geometry. For the cavity in this experiment the geometry factor was calculated to be 4% (point source); this is rather poor. The cavity should be redesigned in such a manner that the source geometry factor could be improved. Some consideration should also be given to keeping the radiation source outside the cavity. Also, in the future, radiation sources should be chosen which will withstand more heat than the type used in this experiment. Actually the cavity could be redesigned easily so that a Woods metal seal would not be necessary, and the heat problem could be resolved in this manner.

A series of investigations should be made to see if the dosimeter could actually be used as a particle detector. This is feasible because there will be step changes in the relative dielectric constant whenever radiation strikes the crystal. This step change in relative dielectric constant would be reflected in a step change in frequency. In experimental run number 4, which used the phase lock loop, this step change in frequency would cause a step change in phase error voltage. The step change in error voltage would be directly proportional to the energy of the radiation striking the crystal. Thus the step change could be differentiated, giving an output whose magnitude would be proportional to the radiation energy. Since the step change in relative dielectric constant could be sensed in a few cycles of the electric field, the time resolution of the instrument would depend solely on the frequency of the electric field. Hence, as the frequency of the field is increased, so is the time resolution of the detector.

This detector would have the same low noise, low energy, and low flux characteristics as the dosimeter explored in the preceding work, but with one exception. If higher frequency electric fields are used, the sensitivity of the device would increase. Also at higher frequencies, microwave cavities could be used. The entire cavity could be filled with the semiconductor and part, if not all, of one wall of the cavity could be removed without appreciably affecting the operation of the microwave cavity. This means that the radioactive source could be kept outside the cavity, and also that there would be no intervening wall between the detector and the radioactive source. Furthermore, the cavity could be made smaller, or the crystal could be made larger with a resulting increase in the stopping power. This would extend the upper energy limit.

Other investigations could follow the lines set down in the preceding paragraphs except that instead of making use of the cumulative photodielectric effect, just the photodielectric effect could be used. Again, if a crystal were placed in a microwave cavity and radiation allowed to fall on it, momentary shifts of the resonant frequency would occur. These shifts would be proportional to the intensity of the radiation, and could be detected using phase angle techniques already discussed. The output voltage of the phase detector would be proportional to the amount of energy. This voltage could be differentiated, and its magnitude would be proportional to the energy present. Note that the resolution of this detector would be limited only by the dead-time of the detector. The dead-time would be limited by the electron-hole pair recombination time. In fact, this time should be short since

there are no DC fields present to keep the electron-holes from recombining. The electron-holes would remain ionized long enough for the dielectric change in the crystal to be sensed by the applied low voltage AC field.

Other methods like the one described by Borisov and Marinov could be investigated further. Thus the three different types of AC mode operation could be used as an improved detector. These types are photoconductive, photodielectric, and cumulative photodielectric.

BIBLIOGRAPHY

1. Arndt, G. D. "Photodielectric Effect of Bulk Semiconductors in Resonant Cavities." Ph.D. Dissertation, The University of Texas, Austin, Texas, 1966.

2. Aven, M. and J. S. Prener. Physics and Chemistry of II-VI Compounds. New York: John Wiley & Sons, 1967.

3. Bethe, H. A. Handbuch der Physik, Vol. 24. Berlin: Julius Springer, 1933.

4. Bethe, H. A. "Bremstormel fur Elektronen Relativistischer Geschwindigkeit." Z. Physik, 76 (1937), p. 293.

5. Boom, M. and M. Hogaboom. Principles of Electroplating and Electroforming. New York: McGraw-Hill, 1936.

6. Borisov, M. and M. Marinov. Dak. Bulg. Akad. Nauk. 11 (1958), p. 169.

7. Bube, R. H. "Comparison of Surface-Excited and Volume-Excited Photoconduction in Cadmium Sulfide Crystals." Phys. Rev. 101 (1956), p. 1668.

8. Bube, R. H. Photoconductivity of Solids. New York: John Wiley & Sons, 1960.

9. Bube, R. H., G. A. Dussel, C. Ho, and L. D. Miller. "Determination of Electron Trapping Parameters." J. Appl. Phys. 37 (1966), p. 21.

10. Cardona, M. and G. Harbeke. "Optical Properties and Band Structure of Wurtzite-Type Crystals and Rutile." Phys. Rev. 137A (1965), p. 1467A.

11. Chase, R. and H. Robinowitz. Principles of Radioisotope Methodology. Minneapolis: Burgess, 1962.

12. Colbow, K. "Free-to-Bound and Bound-to-Bound Transitions in CdS." Phys. Rev. 141 (1966), p. 742.

13. Dearnaley, G. and D. C. Northrop. Semiconductor Counters For Nuclear Radiations. 2 ed. London: E. & F. N. Spon Ltd., 1966.

14. Dussel, G. A. and R. H. Bube. "Electric Field Effects in Trapping Processes." J. Appl. Phys. 37 (1966), p. 2797.

15. Eastman, P. C. and D. E. Brodie. "CdS Films With Adjustable Carrier Density in Any Given Sample." Proc. IEEE 53 (1965), p. 512.

16. Garlick, G. F. J. and A. F. Gibson. "Electron Traps and Dielectric Changes in Phosphorescent Solids." Proc. Roy. Soc. A 188 (1947), p. 485.

17. Hartwig, W. H. "Quantum Detection of Light, Using the Photodielectric Effect in Semiconductors." Bull. Amer. Phys. Soc. 11 (1966), p. 764.

18. Hartwig, W. H. and G. D. Arndt. "Observation of the Photodielectric Effect in Semiconductor Crystals at Low Temperature." Bull. Amer. Phys. Soc. 11 (1966), p. 52.

19. Hartwig, W. H. and J. J. Hinds. "Use of the Photodielectric Effect to Observe Trap Filling in CdS:Ag at 4.2°K." Bull. Amer. Phys. Soc. 13 (1968), p. 168.

20. Harvey, A. I. Microwave Engineering. New York: Academic Press, 1963.

21. Heimbecker, M. A. "A Study of the Feasibility of an A. C. Radiation Detector." Masters Thesis, The University of Oklahoma, Norman, Oklahoma, 1968.

22. Hinds, J. J. "The Photodielectric Effect in Cadmium Sulfide." Masters Thesis, The University of Texas, Austin, Texas, 1968.

23. Hopfield, J. J. and D. G. Thomas. "Fine Structure and Magneto-Optic Effects in the Exciton Spectrum of CdS." Phys. Rev. 122 (1961) p. 35.

24. Howard, R. A. Nuclear Physics. California: Wadsworth Publishing Company, Inc., 1963.

25. Kallman, H. and P. Mark. "De-Excitation of ZnS and ZnCdS Phosphors by Electric Fields." Phys. Rev. 105 (1957), p. 1445.

26. Kittel, C. Introduction to Solid State Physics. 2 ed. New York: John Wiley & Sons, 1968.

27. Kronenberg, S. and C. A. Accardo. "Dielectric Changes in Inorganic Phosphors." Phys. Rev. 101 (1956), p. 989.

28. Kulp, B. A. "Defects in Cadmium Sulfide Crystals." J. Appl. Phys. 36 (1965), p. 553.

29. Kulp, B. A., R. M. Detweiler, and W. A. Anders. "Temperature Dependence on Edge Emission in Single Crystal Cadmium Sulfide." Phys. Rev. 131 (1963), p. 2036.

30. Lambe, John. "CdS With Silver Activator." Phys. Rev. 100 (1955), p. 1586.

31. Lambe, John. "Recombination Processes in CdS." Phys. Rev. 98 (1955), p. 985.

32. Lambe, J. J. and C. C. Klick. "Model for Luminescence and Photoconductivity in the Sulfides." Phys. Rev. 98 (1955), p. 909.

33. Lenard, P. and S. Saeland. "Uber die lichtelektrische und aktinodielektrische Wirkung Beiden Erdalkaliphosphoren." Ann. Phys. 28 (1909), p. 476.

34. Moller, C. "Zur Theorie des Durchgangs schneller Elektronen durch Materie." Ann. Phys. 14 (1932), p. 531.

35. Moreno, T. Microwave Transmission Design Data. New York: Dover Publications, Inc., 1958.

36. Nozieres, P. and D. Pines. "Electron Interaction in Solids, Collective Approach to the Dielectric Constant." Phys. Rev. 109 (1958), p. 702.

37. Nozieres, P. and D. Pines. "Electron Interaction in Solids, General Formulation." Phys. Rev. 109 (1958), p. 741.

38. Nussbaum, A. Electromagnetic and Quantum Properties of Materials. New Jersey: Prentice-Hall, 1966.

39. Pell, E. M. "Ion Drift in an n-p Junction." J. Appl. Physics. 31 (1960), p. 291.

40. Ramo, S. and J. R. Whinnery. Fields and Waves in Modern Radio. 2 ed. New York: John Wiley & Sons, 1953.

41. Rogers, M. The Handbook of Practical Electroplating. New York: McMillan, 1959.

42. Rose, A. Concepts in Photoconductivity and Allied Problems. New York: Interscience Publishers, 1963.

43. Sucker, M. and J. Fox. Handbook of Microwave and Measurements. New York: Interscience Publishers, 1963.

44. Wang, S. Solid State Electronics. New York: McGraw-Hill, 1966.

45. Woodbury, H. H. "Diffusion of Cd in CdS." Phys. Rev. 134A (1964), p. A492.

46. Woods, J. "Changes in Conductivity Resulting From Breakdown in CdS Crystals." Proc. Phys. Soc. 69 (1956), p. 975.

47. Woods, J. and K. H. Nichols. "Photochemical Effects in Cadmium Sulfide Crystals." British J. Appl. Phys. 15 (1964), p. 1361.

APPENDIX I

DESIGN OF PHASE DETECTOR ELECTRONIC CIRCUITS

The output characteristic of the HP 10514A mixer-phase detector is shown in figure A-1. The phase detector puts out a maximum voltage when the two input signals are in phase (0° phase difference) or completely out of phase (180° phase difference.) This signal must first be inverted so that if the cavity is not in resonance, then an error signal is obtained; also at the same time some amplification of the signal can be obtained.

This error signal is then integrated by an operational amplifier, operating as an integrator. This is necessary because the control system must remember what the previous correction voltage was, or the system will oscillate. The integrated voltage is then applied to a transistor amplifier which in turn drives an emitter follower. The oscillator voltage control input requires 0 to -30 volts to drive it, with a nominal impedance of 4K. This load can be supplied by a pnp emitter follower.

Several precautions must be observed. The entire system is a DC amplifier, and DC amplifiers show an inherent tendency to drift. Filbrick 65 AU operational amplifiers have little drift, and are as stable as the power supply. Thus, highly stable power supplies are necessary; and this also applies to the transistor amplifiers. The entire system is temperature dependent, and must be thermally stabilized before it is used.

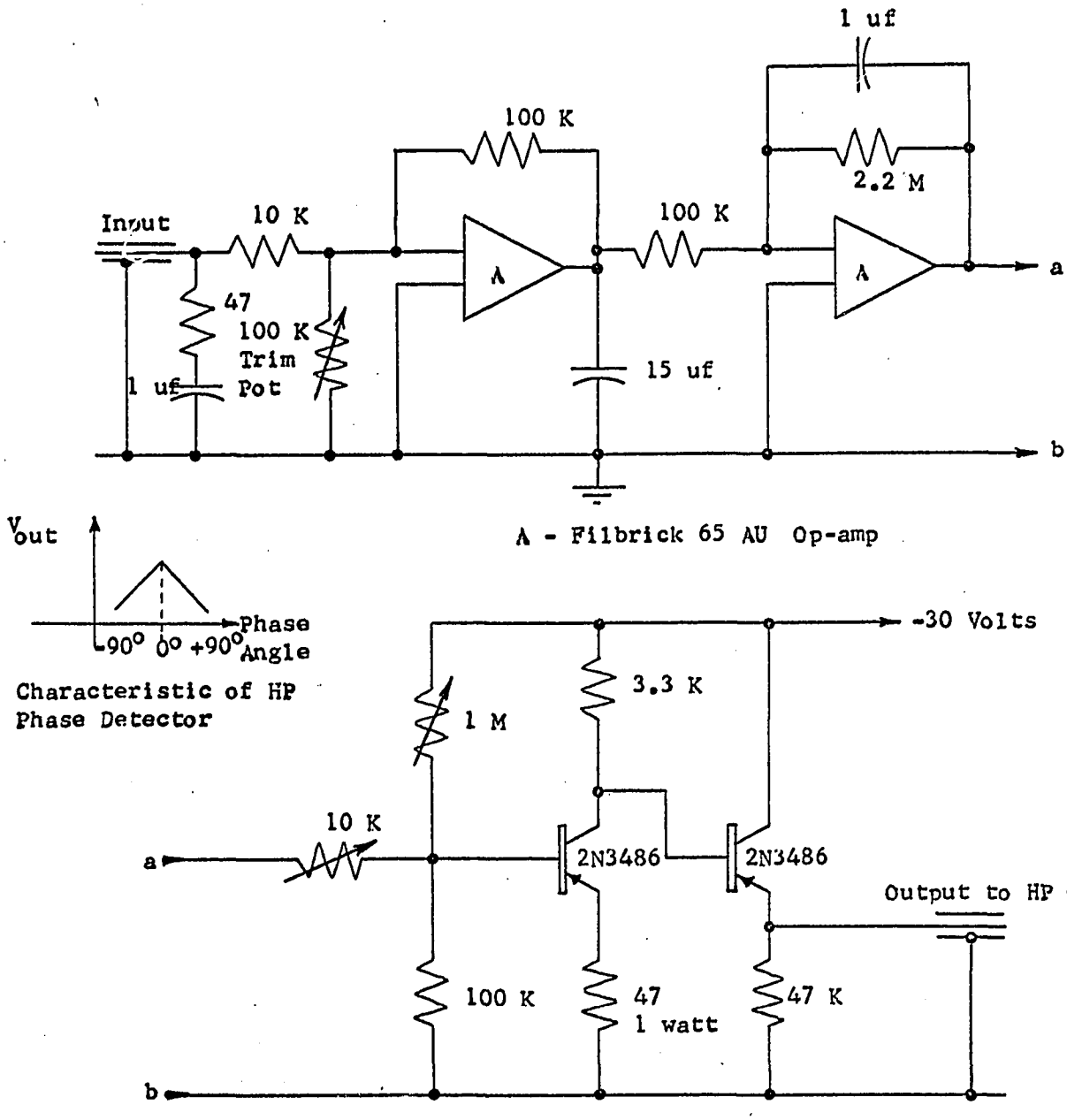

Figure A-1. Phase Detector Electronics

APPENDIX II

TERMINOLOGY

One event-one charge principle.

The ionizing potential for air is roughly 30eV. (This varies from gas to gas). Thus one event gives one charge if the incoming radiation energy is 30eV or greater. The number of ionizing events would be given by E/30eV (for air), where E is the energy of the nuclear radiation .

Gamma ray characteristic.

The gamma ray characteristic of a detector may be defined as the response of the detector to increasing gamma ray energy. (See the figure below).

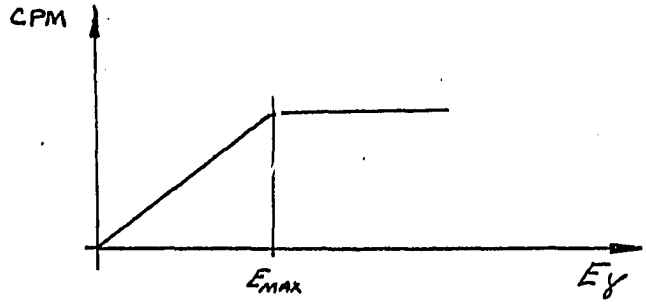

Notice that this characteristic is fairly flat after a certain maximum energy has been reached. This maximum value is the energy resolution cut-off point. (That is, at about this energy, the detector's output is

no longer proportional to the radiation energy.

Effective Mass.

In free space the mass of an electron is determined by measuring the charge to mass ratio e/m, by measuring the deflection of an electron beam in a cathode ray tube. Inside a solid this experiment would have no meaning. The effective mass is a correction term which accounts for electron-electron interactions in a crystal, and applies to equations of motion for an electron in a solid.

Consider first an electron moving in a vacuum whose total energy can be expressed as

$$E = T = \tfrac{1}{2}mv^2 \ . \qquad (A\text{-}1)$$

Using

$$p = mv \qquad (A\text{-}2)$$

this becomes

$$E = \frac{p^3}{2m} \qquad (A\text{-}3)$$

and by using de Broglie's relationship

$$E = \frac{\hbar^2 k^2}{2m} \qquad (A\text{-}4)$$

where $k = 1/\lambda$, the wavelength.

Now differentiate this equation with respect to k.

$$\frac{dE}{dk} = \frac{\hbar^2 k}{m} \ , \qquad (A\text{-}5)$$

and once again

$$\frac{d^2E}{dk^2} = \frac{\hbar^2}{m} \qquad (A\text{-}6)$$

so that the mass of the free electron can be expressed as

$$m = \hbar^2 \Big/ \frac{d^2E}{dk^2} \quad . \qquad \text{(A-7)}$$

This definition may be applied to an electron in the crystal lattice, and determines what is known as the effective mass of an electron.

$$m_e = \hbar^2 \Big/ \frac{d^2E}{dk^2} \quad . \qquad \text{(A-8)}$$

This equation assumes an isotropic crystal; however, if the crystal is anisotropic the equation may be modified, giving rise to the effective mass tensor. Further information may be found in references 26 and 38.